Benefits of High-voltage SiC-based Power Electronics in Medium-voltage Power-distribution Grids*

Fred Wang[1, 2] *and Shiqi Ji*[3*]

(1. Department of Electrical Engineering and Computer Science, The University of Tennessee, TN 37996, USA;
2. Oak Ridge National Lab, Oak Ridge, TN 37830, USA;
3. Department of Electrical Engineering, Tsinghua University, Beijing 100084, China)

Abstract: Medium-voltage (MV) power electronics equipment has been increasingly applied in distribution grids, and high-voltage (HV) silicon carbide (SiC) power semiconductors have attracted considerable attention in recent years. This paper first overviews the development and status of HV SiC power semiconductors. Then, MV power-converter applications in distribution grids are summarized and the benefits of HV SiC in these applications are presented. Microgrids, including conventional and asynchronous microgrids, that can fully demonstrate the benefits of HV SiC power semiconductors are selected to investigate the benefits of HV SiC in detail, including converter-level benefits and system-level benefits. Finally, an asynchronous microgrid power-conditioning system (PCS) prototype using a 10 kV SiC MOSFET is presented.

Keywords: Silicon carbide power semiconductor, distribution grid, asynchronous microgrid, power-conditioning system

1 Introduction

Many applications have been proposed, developed, and/or implemented for power electronics converters in medium-voltage (MV, 1-35 kV ac) distribution grids. Power electronics have been employed in custom power equipment, including power-flow control [1-3] (e.g., solid-state transfer switch, solid-state circuit breaker, and fault-current limiter), power conditioning [4-6] (e.g., static synchronous compensator, dynamic voltage restorer, and unified power quality conditioner) and active power filtering [7]. More recent power electronics applications include renewable energy interface converters [8-12] (e.g., solar photovoltaic and wind turbine), energy-storage systems [13-17] (e.g., battery and flywheel), and microgrid interface converters (for both ac and dc microgrids) [18-22]. There are also some other emerging applications for power electronics, such as solid-state transformers [23-26], controlled network transformers [27], and continuously variable series reactors [28]. In summary, more and more power converters are needed in MV distribution grids. Because many of these applications are high power (hundreds of kilowatts to tens of megawatts), it is often more advantageous to use MV converters. The power semiconductor is a key enabler for such MV power converters.

Most current MV power converters are based on Si power semiconductors (e.g., Si IGBT). In recent years, high-voltage (HV) silicon carbide (SiC) power semiconductors, typically referring to device voltage ratings of 3.3 kV or higher, are being rapidly developed [29-54]. As wide-bandgap (WBG) semiconductor devices, SiC power devices have many advantages over their Si counterparts, including (1) a higher breakdown electric field, and therefore lower specific on-resistance and higher

Manuscript received December 1, 2020; revised January 4, 2021; accepted March 2, 2021. Date of publication March 31, 2021; date of current version March 8, 2021.
* Corresponding Author, E-mail: sxjisq@gmail.com
* Supported by the DOE through Oak Ridge National Lab and the Power America Program, the Engineering Research Center Program of the National Science Foundation, and the CURENT Industry Partnership Program.
Digital Object Identifier: 10.23919/CJEE.2021.000001

voltage rating (e.g., up to 15 kV for unipolar devices and >20 kV for bipolar devices compared to the maximum voltage of 6.5 kV for Si IGBT); (2) a faster switching speed, and therefore lower switching loss and higher switching frequency; and (3) better thermal performance.

By using HV SiC power semiconductors, the benefits of MV power converters can be realized in several ways. (1) Direct device substitution: A direct substitution using SiC devices can lead to gains in efficiency and corresponding reduce need for cooling. (2) Topology simplification: HV SiC devices have higher breakdown voltages than Si devices. In addition, SiC devices can switch much faster and have lower switching loss than Si devices. As a result, the converter topology can be simplified (e.g., using simpler hard-switching topology). (3) New and/or enhanced functionality/applications: With high switching speed and frequency, HV SiC devices can enable MV power converters with higher control bandwidth and faster dynamic response. These features can lead to new or enhanced functionalities in existing applications, or even new applications. These benefits are discussed in detail.

In this paper, the HV SiC devices are surveyed in Section 2. In Section 3, MV power electronics equipment in distribution grids are summarized, and the benefits of SiC in these applications are introduced. The microgrids, including conventional microgrid and asynchronous microgrid, are selected as an example for detailed investigation in Sections 4 and 5, respectively. A 10 kV SiC MOSFET-based PCS prototype is demonstrated in Section 6.

2 Review of HV SiC power semiconductors

Nowadays, HV (>3.3 kV) Si power devices such as SCR thyristors, gate turnoff thyristors (GTO), gate-commutated thyristors (GCT), and insulated-gate bipolar junction transistors (IGBT), have reached a zenith of development due to Si's physical material limits [29-30]. The voltage capability of Si devices is typically below 6-12 kV and, more importantly, the switching frequency capability is normally less than 1 kHz for these HV devices. Moreover, the junction temperatures are usually kept below 125 ℃, which poses a cooling challenge and limits their applications in certain harsh environments [29].

2.1 General characteristics

Breakthroughs in WBG SiC material and fabrication technology have led to the development of HV, high-frequency power devices [31]. SiC exists in a variety of polymorphic crystalline structures called polytypes, e.g., 3C-SiC, 6H-SiC, 4H-SiC. Presently 4H-SiC is generally preferred in practical power device manufacturing for its higher carrier mobility and lower dopant ionization energy [32]. Tab. 1 compares the main characteristics between 4H-SiC and Si at 300 K. Compared with HV Si devices, some benefits of SiC devices can be drawn based on the electrical properties.

Tab. 1 Comparison of electrical properties of Si and 4H-SiC

Material property	Si	4H-SiC
Energy bandgap E_G/eV	1.12	3.26
Breakdown field E_B/(V/cm)	2.5×10^5	2.2×10^6
Thermal conductivity/(W/cm • ℃)	1.5	4.9
Saturation drift velocity v_s/($\times10^7$cm/s)	1.0	2.1

2.1.1 Lower specific on-resistance

With a breakdown field 10 times higher than that of Si, a thinner drift layer (0.1 times that of Si devices) with a higher doping concentration (more than 10 times higher) can be used for SiC power devices at the same blocking voltage [33-34]. For unipolar devices, such as Schottky diodes and MOSFETs, the combination of thinner blocking layer and higher doping concentration yields a lower specific on-resistance compared with Si majority-carrier devices.

2.1.2 Faster switching speed

Two factors contribute to fast switching characteristic in SiC devices, higher breakdown voltage and higher saturated drift velocity. First, with lower on-resistance at the same breakdown voltage, a smaller chip size is achieved in SiC unipolar devices such as MOSFETs. Therefore, the capacitance is smaller due to the reduced size, and a fast switching speed is realized. For minority carrier conductivity modulated devices such as PiN diodes or IGBTs, as the diffusion length (required to modulate the conductivity of the blocking layer) is reduced, thus resulting in a faster switching speed

in SiC IGBTs. Second, minority carriers are swept out of the depletion region at the saturated drift velocity during the turn-off transient. Because the electron saturated drift velocity of 4H-SiC is twice the saturated drift velocity of Si, a higher saturated drift velocity increases the SiC device switching speed.

2.1.3 Higher current density and temperature

The thermal conductivity of SiC is more than 3 times that of Si. Higher thermal conductivity allows the dissipated heat to be readily extracted from the device. Hence, greater power can be applied to the device at a given junction temperature. Also, the higher thermal conductivity together with the wide bandgap makes it possible for the SiC device to work in high-temperature applications.

2.2 HV SiC characteristics

After intensive development, low-voltage (600 V, 1 200 V, and to some extent, 1 700 V) SiC devices are becoming commercially available, and have started to be applied in commercial products. On the other hand, the HV SiC are generally in developmental stages with very limited commercial availability and generally small current ratings. This section summarizes the available information on HV SiC devices and modules from Wolfspeed/Cree, GenSiC, USCi, and Fuji. Tabs. 2-4 summarize the key characteristics of devices, including voltage/current ratings and the static and dynamic characteristics.

Tab. 2 Summary of HV SiC diodes

Voltage/Current	Static	Dynamic
10 kV/10 A JBS diode (Wolfspeed [35])	4 V @ 10 A	t_{rr}=365 ns, Q_{rr}=0.84 μC @ 3.15 A
10 kV/50 A 4H-SiC PiN diode (Wolfspeed [36])	3.9 V @ 50 A 5.9 V @ 328 A	t_{rr}=200 ns, di/dt=330 kA/s @ 10 kV/20 A
12.9 kV SiC PiN diode (GeneSiC [37])	3.3 mΩ • cm^2 @ 25 ℃	Not given (NG)
10 kV SiC PiN diode (GeneSiC [37])	5.75 mΩ • cm^2 @ 25 ℃	t_{rr}=250 ns, Q_{rr}=1.67 μC @ 2.4 kV/24 A
10 kV/2 A SiC JBS diode (GeneSiC [37])	114.7 mΩ • cm^2 @ 25 ℃	NG
10 kV/7 A SiC JBS diode (GeneSiC [37])	127.5 mΩ • cm^2 @ 25 ℃	NG
3.3 kV/50 A SiC JBS diode (USCi [38])	2.3 V	NG
6.5 kV/15 A SiC JBS diode (USCi [38])	3.8 V	NG
8 kV/5 A SiC JBS diode (USCi [39])	4.0 V	NG

Tab. 3 HV SiC unipolar devices (MOSFET and JFET**)**

Voltage/Current	Static	Dynamic
Gen-3 MOSFET 3.3 kV /25 A (Wolfspeed [40])	10.6 mΩ • cm^2 @ V_{gs}=20 V	E_{on}=0.70 mJ, E_{off} =0.63 mJ @ 1.8 kV/ 25 A, 25 ℃
Gen-3 MOSFET 3.3 kV /45 A (Wolfspeed [41])	45 mΩ @ V_{gs}=20 V, 25 ℃	E_{total} = 1.1 mJ @ 1.8 kV/ 20 A, 25 ℃
3.3 kV improved Gen-3 MOSFET (Wolfspeed [41])	40 mΩ @ V_{gs}=20 V, 25 ℃	NG
10 kV/5 A DMOSFET (Wolfspeed [42])	111 mΩ • cm^2 @ V_{gs}=15 V, 25 ℃	E_{on}=240 μJ, E_{off} =50 μJ @ 1.0 kV/3 A,
Gen-3 MOSFET 6.5 kV /30 A (Wolfspeed [41])	100 mΩ @ 25 ℃	NG
10 kV/10 A MOSFET (Wolfspeed [35])	127 mΩ • cm^2 @ V_{gs}=20 V, 25 ℃	E_{on}=4.48 mJ, E_{off}=0.81 mJ @ 5.3 kV/10 A
Gen-3 MOSFET 10 kV /20 A (Wolfspeed [40])	86 mΩ-cm^2 @ V_{gs}=20 V	E_{on}=6.5 mJ, E_{off}=1 mJ @ 6 kV/20 A
10 kV enhanced short circuit Gen-3 MOSFET (Wolfspeed [41])	350 mΩ @ V_{gs}=20 V	E_{total}=21 mJ @ 7 kV/15 A
Gen-3 MOSFET 15 kV /10 A (Wolfspeed [44])	208 mΩ • cm^2 @ V_{gs}=20 V	E_{on}=4.8 mJ, E_{off}=1 mJ @ 6 kV/10 A,
6.5 kV/15 A normally off JFET (USCi [48])	350 mΩ @ 25 ℃	E_{on}=2.71 mJ, E_{off}=1.54 mJ @ 3 kV/11 A
6.5 kV super cascode JFET (USCi [49])	230 mΩ @ 25 ℃	E_{on}=1.2 mJ, E_{off}=0.53 mJ @ 3 kV/11 A
3.3 kV/180 A MOSFET half-bridge module (Wolfspeed [41])	11.3 mΩ @ 25 ℃	E_{total}=45 mJ @ 2.2 kV/180 A, 25 ℃
10 kV/240 A MOSFET half-bridge module (Wolfspeed [41])	19.4 mΩ	NG
6.5 kV/60 A JFET half-bridge module (USCi [39, 48])	100 mΩ @ 25 ℃	E_{on}=28 mJ, E_{off}=9.2 mJ @ 3 kV/60 A, 25 ℃
6.5 kV/400 A MOSFET half-bridge module (Mitsubishi [50])	20 mΩ @ 175 ℃	E_{on}=0.41 J, E_{off}=0.11 J @ 3.6 kV/400 A, 175 ℃
3.3 kV/750 A MOSFET half-bridge module (Mitsubishi [51])	5.7 mΩ @ 175 ℃	E_{total}=0.55 J @ 1.8 kV/600 A, 175 ℃
3.3 kV MOSFET half-bridge module (Toshiba [52])	NG	NG
3.3 kV/200 A MOSFET half-bridge module (Fuji [53])	14 mΩ @ 150 ℃	NG
3.3 kV/750 A MOSFET half-bridge module (Fuji [54])	5 mΩ @ 150 ℃	E_{on}=0.52 J, E_{off}=0.41 J @ 1.5 kV/750 A, 150 ℃

Tab. 4 HV SiC bipolar devices (IGBT, BJT and thyristor**)**

Voltage/Current	Static	Dynamic
12 kV/0.5 A p-IGBT (Wolfspeed [45])	18.6 mΩ • cm^2 @ 25 ℃	t_{on}=40 ns, t_{off}=2.8 μs @ 1.5 kV/0.55 A
12.5 kV/35 A n-IGBT (Wolfspeed [46])	5.3 mΩ • cm^2 @ 32 A, 25 ℃	t_{off}=0.65 μs @ 5 kV/5 A 25 ℃, w/2 um F-S buffer
15 kV/20 A p-IGBT (Wolfspeed [34])	6.5 V @ 20 A, 25 ℃	NG
15 kV/20 A n-IGBT (Wolfspeed [34])	7.0 V @ 20 A, 25 ℃	NG
16 kV flip-type n-IGBT (Fuji [47])	6.5 V @ 20 A	NG
22.6 kV/20 A n-IGBT (Wolfspeed [34])	NG	NG
10 kV/8 A BJT (GeneSiC [37])	110 mΩ • cm^2	E_{on}=4.2 mJ, E_{off}=1.6 mJ @ 5 kV/8 A
6.5 kV Thyristors (GeneSiC [37])	2.8 mΩ • cm^2	dv/dt=1 920 V/μs @ 3.6 kV/14.5 A

For the active switches, HV SiC MOSFETs are the most developed with some IGBTs, BJTs, and

thyristors also available. From Tab. 3 and Tab. 4, it can be seen that the advantage of IGBTs over MOSFETs is very limited. In the Si case, the IGBT is more advantageous beyond 600 V to 1 000 V than the MOSFET. For SiC, the trend should hold, but probably at much higher voltages; that is, perhaps at higher voltages (>15 kV), the SiC IGBT is superior to the SiC MOSFET. In this paper, we primarily focus on SiC MOSFETs. For HV diodes, as compared to PiN diodes, the Schottky diode has poor static performance and large conduction loss, but has excellent reverse recovery characteristics. Also, considering that MOSFETs are capable of operating in the third quadrant, the HV SiC Schottky diode is selected as the anti-parallel diode of the SiC MOSFET for later comparison.

Fig. 1 shows the relationship between the specific on-resistance and device breakdown voltage for various SiC MOSFETs, including low-voltage (LV) devices [40]. It can be seen that the HV SiC MOSFET characteristics closely follow the SiC material 1-D limit, indicating that the on-resistance is dominated by the drift layer resistance for these devices. Since the specific on-resistance $R_{on,\ sp}$ is proportional to the square of the breakdown voltage for the 1-D limit, the lower-voltage devices have lower normalized resistances. For example, $R_{on,\ sp}$ of a 6.5 kV device is roughly 4 times that of a 3.3 kV device.

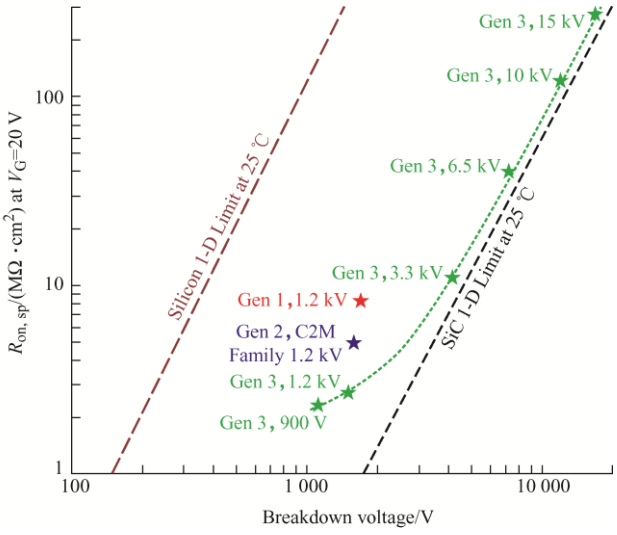

Fig. 1 Specific on-resistance as function of breakdown voltage

3 MV power converters in distribution grids

The existing and emerging power electronics-based equipment for MV distribution grids, including today's and future grids, are summarized in this section. The equipment can include the following categories: (1) "traditional" custom power equipment, including equipment for power-flow control (e.g., solid-state transfer switch, solid-state circuit breakers and fault-current limiters), power conditioning (e.g., STATCOM, dynamic voltage restorer, unified power quality conditioner) and active power filtering; (2) emerging equipment, including renewable energy interface converters, energy-storage/charging converters, microgrid interface converters (for both dc and ac) and microgrids; (3) some more recent variations of traditional equipment to address the size, cost, controllability, reliability, and issues associated with high penetration of renewable energy sources, including solid-state transformer, controlled network transformer and continuously variable series reactor.

3.1 "Traditional" custom power equipment

Owing to better controllability and faster dynamic response over traditional electrical equipment, the power electronics-based equipment can improve the performance of the conventional distribution grid. Like flexible ac transmission systems (FACTS), the term custom power (CP) pertains to the use of power electronics controllers for distribution systems. Just as FACTS improves the reliability and quality of power transmission by simultaneously enhancing both power transfer capability and stability, the custom power enhances the quality and reliability of power delivered to customers. There are many different types of custom power equipment, which can be grouped into three categories, namely, power-flow control/ interruption devices, power conditioning and compensation devices, and active harmonic filters.

3.1.1 Power-flow control/interruption

In this case, the power electronics equipment is used as the switch and can replace the conventional mechanical switches for power-flow control and interruption. Several equipment types developed are solid-state transfer switch (SSTS), solid-state circuit breaker (SSCB), and solid-state fault-current limiter (SSFCL), as shown in Fig. 2.

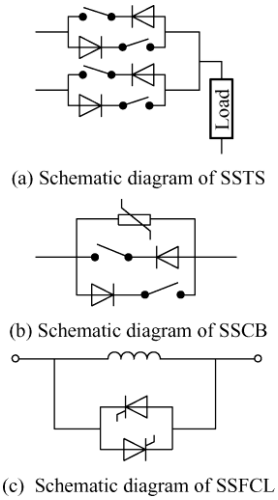

(a) Schematic diagram of SSTS

(b) Schematic diagram of SSCB

(c) Schematic diagram of SSFCL

Fig. 2 Power-flow control and interruption equipment

Many industrial and commercial operations suffer from various types of outages and service interruptions that can cost significant financial loss per incident in terms of lost production, process down-time, and other tangible effects. A SSTS can be one of the most cost-effective solutions for these types of power quality problems [1]. The SSTS, which essentially consists of a pair of bidirectional thyristors, enables seamless transfer of energy from a primary source to an alternate source, thus avoiding service interruption upon the detection of a power-quality deficiency. The typical schematic diagram is shown in Fig. 2a. Both pure SSTS and hybrid transfer switch with SSTS and mechanical switch were developed. The hybrid transfer switch shows benefits in power-loss reduction while pure SSTS has better performance in switching dynamics.

SSCB can replace the conventional mechanical circuit breaker to achieve a faster dynamic response. Furthermore, the SSCB can be used to interrupt a dc current that does not have a zero-current crossing and is essential for a dc grid. The typical schematic diagram is shown in Fig. 2b. Both pure SSCB and hybrid circuit breaker with SSCB and a mechanical breaker were developed. The mechanical switch is slow, and the semiconductor switch is lossy. The hybrid dc circuit breaker can achieve both low loss and fast breaking time, which is the trend for future dc breaker development [2].

The typical schematic diagram of SSFCL is shown in Fig. 2c. In normal operation, the solid-state switch turns on and the impedance of FCL is nearly zero. When a fault occurs, the switch turns off and current flows through an inductor and the fault current is limited. In recent years, many types of SSFCL, such as series switch type, bridge type, and resonant type, were developed based on SCR, GTO, IGCT, and IGBT [3].

3.1.2 Power system conditioning and compensation

The power system conditioning and compensation equipment is applied to improve the quality of the power delivered to electrical load equipment by regulating voltage and compensating reactive power. In conventional distribution grids, these functions are achieved mainly by passive components, such as inductors, capacitors, and tap-changing transformers. In order to improve the controllability of the grid, power electronics equipment has been developed to replace the passive components as conditioning and compensation devices [4-5]. Based on their connection schemes in the distribution lines, these conditioning and compensation devices can be categorized into several types [6], as shown in Fig. 3, including distribution static synchronous compensator (DSTATCOM), dynamic voltage restorer (DVR), and unified power quality conditioner (UPQC).

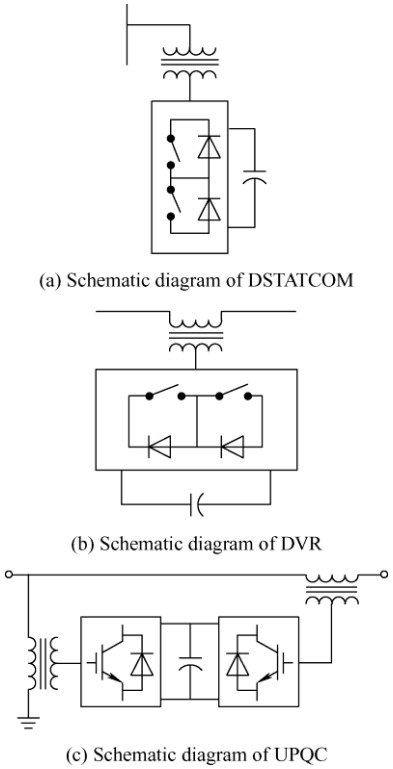

(a) Schematic diagram of DSTATCOM

(b) Schematic diagram of DVR

(c) Schematic diagram of UPQC

Fig. 3 Power system conditioning and compensation equipment

The DSTATCOM is shunt connected with the distribution grid, often through a transformer, as

shown in Fig. 3a. DSTATCOM is generally based on voltage-source converters (VSCs) and can control the reactive power output through controlling the reactive current injected into the distribution grid.

The DVR is series connected with the distribution line, as shown in Fig. 3b. The function of DVR is similar to that of DSTATCOM, which compensates for voltage sags and voltage swells, but unlike the operation of DSTATCOM, it is designed to inject a dynamically controlled voltage. The controllable converter is also generally a VSC.

The UPQC is a combination of DSTATCOM and DVR, as shown in Fig. 3c. An UPQC comprises of two PWM-controlled converters that use one common dc bus. Two parameters, a shunt current and series voltage, are used as reference for the control. In addition to achieving the benefits of the DSTATCOM and DVR, UPQC allows real power exchange between the shunt- and series-connected VSCs, leading to more benefits.

3.1.3 Active power filter

An active power filter (APF) works as a controlled current source to compensate for the harmonic currents in the grid, as shown in Fig. 4. APFs can be categorized as shunt-connected, series-connected APF and hybrid-connected APF, according to their connections in a grid [7]. Their topologies are very similar to those of compensators.

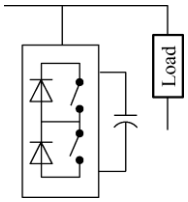

Fig. 4 Schematic diagram of APF

3.2 Emerging applications

This section deals with the emerging power electronics applications at the distribution level, i.e., those associated with distribution energy resources (DER), including photovoltaic (PV), wind, battery and flywheel energy-storage, micro-turbines, and fuel cells. Many of the DERs are included in emerging in microgrids. Therefore, microgrids, including ac microgrids, dc microgrids, and asynchronous microgrids, are also covered.

3.2.1 Renewable energy systems

PV technology involves converting solar energy directly into electrical energy by means of a solar cell. For a PV system, the voltage output is a constant dc whose magnitude depends on the configuration in which the solar cells/modules are connected. The main requirement of power electronic interfaces for the PV systems is to convert the generated dc voltage into a suitable ac voltage for consumer use or utility connection. Generally, the dc voltage magnitude of the PV array is required to be boosted to a higher level by using dc-dc converters and then, the dc-ac inverters are utilized to convert the voltage to 50/60 Hz ac at standard voltage levels. The most common operating mode for PV system is maximum power point tracking (MPPT). The MPPT control process and the voltage boosting are usually implemented in the dc-dc converter, whereas the dc-ac inverter is used for grid-current control [8]. For PV converters in distribution grids, among the commercial products, the string topology is the most commonly used configuration [9]. For a string converter, several PV panels are connected in series to form a PV string, and each string is connected to interface converter, as shown in Fig. 5.

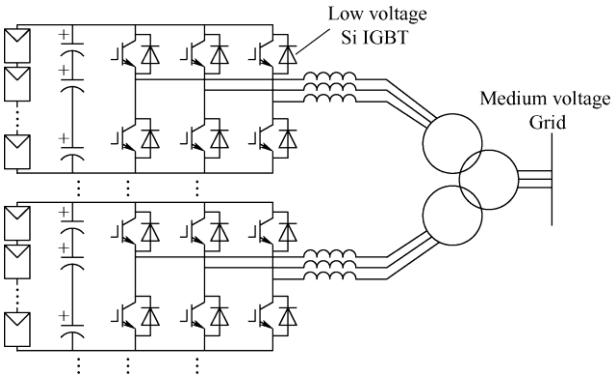

Fig. 5 Configuration of PV string converter

There are four types of wind turbine generators (Types 1 through 4). Most modern wind turbine generators are Types 3 and 4, which involve power electronics converters and have the ability to perform voltage or reactive power control, similar to synchronous machines [10]. Common control modes include constant power factor control, coordinated control across a wind farm to maintain a constant interconnection point voltage, and constant reactive power control [11]. Type 3 is also called doubly fed

induction generator (DFIG), which uses a partial power converter; and Type 4 uses synchronous generator with a full power converter. The configurations of Type 3 and Type 4 wind turbine generators are shown in Fig. 6. Considering the existing products of MV wind converters, the frequently used configurations include two-level, three-level neutral point clamped (3L-NPC) converter, and cascaded H-bridge (CHB) converter.

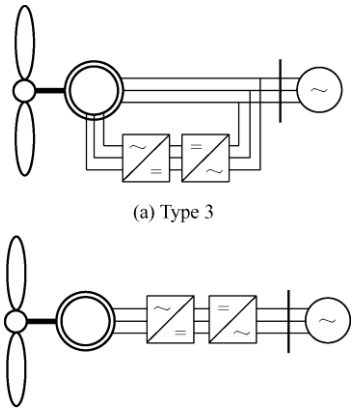

(a) Type 3

(b) Type 4

Fig. 6 Configuration of wind turbines

Considering the existing complex converter topology (e.g., multiple parallel connected in PV and three-level and multi-level in wind turbine [12]) and the bulky 50/60 Hz transformer, HV SiC device can be employed to simplify the topology and increase the power density of the whole system. With the high switching frequency of SiC devices, the ac filter size can be reduced, further improving the system's power density.

3.2.2 Energy-storage system

There are a variety of technologies that can be used to store energy on the utility power system, including batteries, superconducting magnetic energy storage (SMES), flywheels, electrochemical capacitors, compressed air energy storage (CAES), pumped hydro, and production and storage of gases such as hydrogen (to run fuel cells or hydrogen internal combustion engines). Of these technologies, batteries and flywheels are commonly integrated at the distribution system level and are commercially available.

Batteries produce a dc voltage that must be converted to ac to connect to the utility grid. The individual battery cells are generally connected in different configurations in series and/or parallel to achieve the required voltage and current outputs. The power-conditioning systems, including inverters and dc-dc converters, are often required for the battery energy-storage systems (BESS). The unique aspect to power electronics for energy storage is that they must be bidirectional, that is both taking power (during charging) and providing power (during discharge) from/to the grid [13-14]. The simplest form of BESS configuration, as shown in Fig. 7, consists of a battery system followed by a dc-ac inverter. If isolation or a high ratio of voltage conversion is required, a transformer is usually integrated into the system. The current at full operating power determines the rating of the inverter. The current, in turn, is dependent on the BESS voltage at full operating power, which varies substantially from no load to full load. One drawback for this configuration is that the low-frequency transformer (LFT) placed at the output of the inverter makes the system bulky and possibly expensive. With HV SiC devices, the bulky and lossy LFT can be replaced by a lighter and more efficient high-frequency transformer.

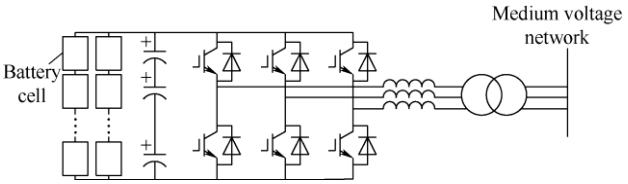

Fig. 7 Configuration of BESS

Flywheel energy-storage system (FESS) stores energy in the form of the kinetic energy of a spinning mass [15]. Conversion from kinetic to electric energy is accomplished by electric machines. FESS utilizes power electronics that convert and regulate the power output from the flywheel. The major electrical components of a flywheel energy-storage system include a bidirectional inverter (Converter 2) and variable-speed motor drive (Converter 1 plus motor/generator) as shown in Fig. 8. The FESS can be classified into two categories. The first technology is based on low-speed flywheels (up to 6 000 r/min) with steel rotors and conventional bearings. The second involves more recent high-speed flywheel systems (up to 60 000 r/min) that are available commercially and make use of advanced composite wheels with much higher energy and power density than steel wheels [16].

Due to the high speed of the motor in flywheel systems, the switching frequency of converter 1 is required to be high. An induction machine-based FESS, which consists of a 20 kHz high-frequency back-to-back pulse density modulated (PDM) converter, was developed [17]. Therefore, SiC devices are very attractive in the FESS due to its high switching frequency capability.

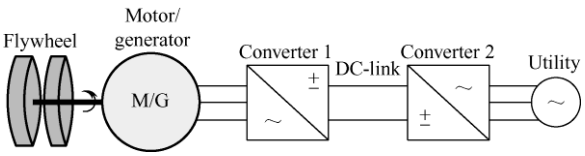

Fig. 8 Configuration of flywheel

3.2.3 Microgrid

The microgrid [18] has been proposed as a solution to integrating DERs without disrupting the operation of the utility grid. The microgrids can even provide ancillary services such as local voltage control. During disturbances on the main grid, microgrids can island and continue to operate autonomously. As a result, microgrids can improve reliability and power quality. Microgrids can be categorized into ac microgrids and dc microgrids depending on the microgrid voltage types [19], as shown in Fig. 9.

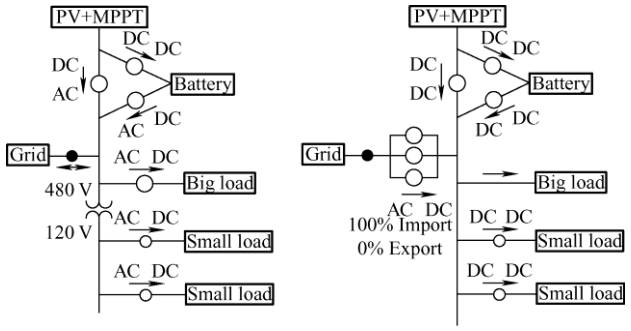

Fig. 9 Architecture of microgrid

The asynchronous microgrid through a power-conditioning system (PCS) has been proposed and promoted recently [20-21]. A typical architecture of asynchronous microgrid is shown in Fig. 10. The asynchronous microgrid has two features: (1) it can decouple the conventional ac microgrid from the utility distribution grids with the PCS, and (2) considering the dc link of the PCS can be used to interface DERs, the asynchronous microgrid could be a hybrid microgrid that comprises a dc link and ac microgrid. Some studies have shown the benefits of asynchronous microgrids in power quality, power loss, operation in transitions, and short circuit. The converter control in the asynchronous microgrid has been studied as well [22].

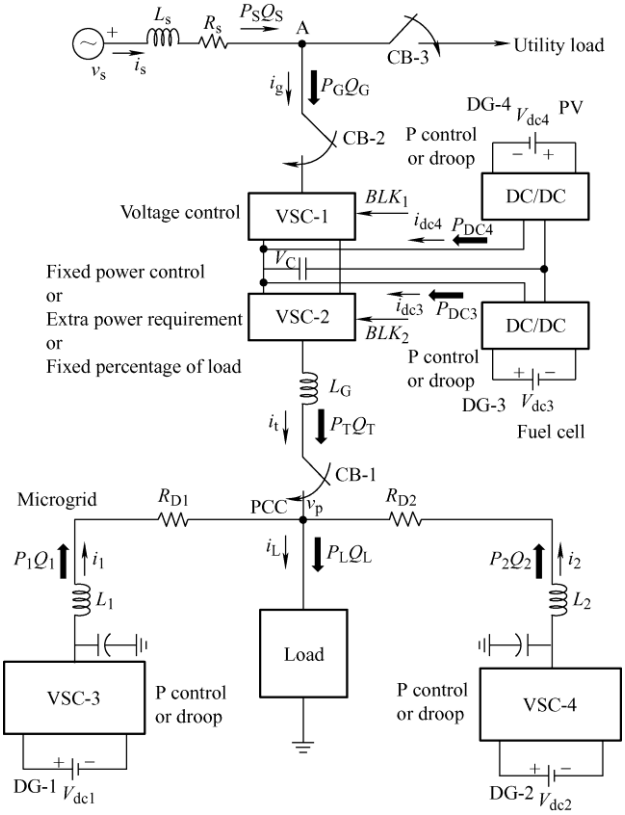

Fig. 10 Architecture of asynchronous microgrid

3.3 Other recent developments

The traditional power electronics-based custom power equipment has limited applications in distribution grids mainly due to their cost and reliability concerns. Some more recent variations have been developed to address these issues, as well as to improve density, controllability and easy integration with the renewable energy sources. The equipment in this category includes solid-state transformer, controllable network transformer and continuously variable series reactor.

3.3.1 Solid-state transformer

With the development of high-voltage, high-frequency power semiconductor devices (e.g., SiC device) and high-frequency magnetic materials, the solid-state transformer (SST) was proposed to replace conventional transformers in some applications [23]. The configuration of SST is shown in Fig. 11. Compared to conventional transformers, the

SST has reduced weight and size and provides flexible controllability. The SST has shown significant benefits over conventional transformers in traction system and smart grids [24].

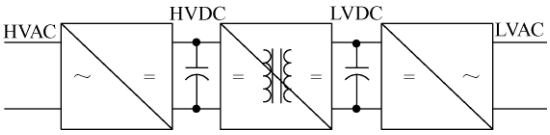

Fig. 11 Configuration of SST

The ABB's medium-frequency transformer (MFT)-based converter system for locomotives [25] weighs 4 500 kg, and the specific power density of its front-end MFT and rectifier is 0.5-0.75 kVA/kg. For a comparable conventional system, the specific power density of the front-end LFT and rectifier is 0.2-0.35 kVA/kg. Therefore, the power density has been more than doubled. With the HV SiC-based MFT, the power density improvement is expected to be even higher. A 1 MW, 4 160 VAC/ 1 000 VDC converter with a 40 kHz isolation transformer using Wolfspeed 10 kV SiC MOSFET, has been designed and built by GE. This prototype unit has a weight of 900 kg, which is approximately 10% of the 60 Hz transformer-rectifier unit used currently. The volume is also reduced to a third of the existing unit [26].

All applications can make use of SST to replace the LFT for significantly improved power density while maintaining high efficiency. Due to the high requirement for the switching frequency in SST, HV SiC can play a major role in the development of this technology.

3.3.2 Controllable network transformer

The controllable network transformer (CNT), as shown in Fig. 12, can achieve the power-flow control through providing simultaneous control of bus voltage magnitudes and phase angles by augmenting an existing load tapped transformer with a small converter [27]. The load tapped transformer has two taps at (1+N) p.u. and (1–N) p.u.. By controlling the switches using a fixed duty cycle, the voltage magnitude of the output voltage can be varied between (1+N) p.u. and (1–N) p.u.. One way to achieve output voltage phase angle control is by using the dual virtual quadrature sources technique. It has been shown that if an even harmonic is introduced in the duty cycle, the phase of the output fundamental voltage can be shifted and controlled. The resulting output voltage consists of a third (or an odd) harmonic component in addition to the phase shifted fundamental component. In this way, the active and reactive power can both be controlled by the CNT.

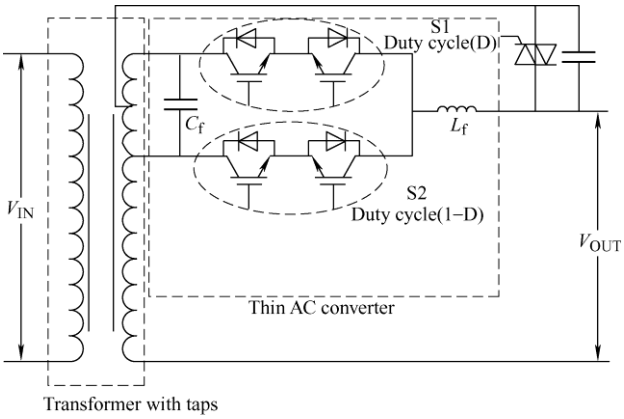

Fig. 12 Schematic diagram of CNT

3.3.3 Continuously variable series reactor

The continuously variable series reactor (CVSR), as shown in Fig. 13, can be used to control power flow through regulating impedance in grids [28]. The ac winding is the controlled element, which can be connected to an ac line; the dc current controller is the controlling element for CVSR through the dc winding, which can vary dc bias flux as well as the magnetization level of the saturable core. As a result, the ac reactance reaches the maximum value when the bias dc flux equals to zero, and the minimum value when the core is fully saturated. The dc current controller is realized through a power electronics converter with a rating of only a small fraction of the ac winding.

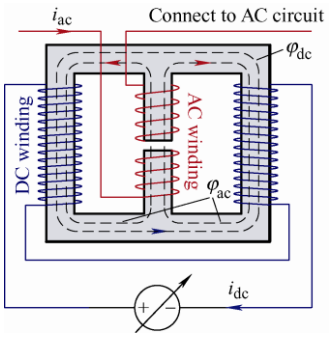

Fig. 13 Schematic diagram of CVSR

3.4 Potential benefits of HV SiC devices

There are in general three ways that WBG devices such as SiC can benefit any applications:

direct device substitution, topology simplification, and new or enhanced functionality or even new applications. In particular, HV SiC devices can benefit MV applications including distribution grids applications the same ways. They are briefly described here.

3.4.1 Direct device substitution

Due to lower power loss of SiC devices over Si devices, a direct substitution using SiC devices can lead to gains in efficiency and corresponding reduced need for cooling. All equipment could benefit from this to some extent.

3.4.2 Topology simplification

HV SiC devices have high breakdown voltages than Si and LV SiC devices. In addition, SiC devices can switch much faster than Si counterparts. As a result, some converter design can be simplified, especially, those topologies requiring many series/paralleled Si devices or many voltage levels to achieve needed system voltage or needed equivalent switching frequency. Most power electronics converters for MV applications exceed the voltage capabilities of the available Si devices (e.g., the highest Si IGBT voltage is 6.5 kV). In addition, the HV Si devices have limited switching capabilities (e.g., the 6.5 kV Si IGBT normally switches at about 1 kHz or less), resulting in low control bandwidth and large pulsating ripple or energy. As a result, multi-level converters, paralleled converters, and/or large passive components for filtering and energy storage are needed. With faster switching and higher voltage rating HV SiC devices, the need for complex topology and large filter can be alleviated. The topology simplification should lead to a lower cost, higher reliability, and high power density.

3.4.3 New and enhanced functionality/applications

With high switching speed and frequency, HV SiC devices can enable MV power converters with higher control bandwidth and faster dynamic response. These features can lead to new or enhanced functionality in existing applications or even new applications.

With regard to traditional custom power equipment, there are mainly three benefits by using HV SiC devices, including the following. (1) The APF functions can be integrated into power conditioning and compensation equipment, given the switching frequency can be considerably higher than harmonic frequencies. The integration can reduce the need for dedicated APF, leading to lower overall converter ratings and cost. (2) For interruption equipment like SSTS, SSCB and SSFCL, HV SiC device can potentially speed up the response time and improve system reliability and reduce cost for passive energy-storage components. (3) The high control bandwidth could enable the equipment to be used in stabilizing the system.

For emerging equipment, mainly the DER interface converters, the benefits pf HV SiC, especially through device substitution and enabling new functionality are achievable. For microgrids that involve DERs and traditional custom power equipment, the benefits of HV SiC can potentially be realized in all three ways. Furthermore, there are more requirements for microgrids and their DERs, such as operation in different modes (grid-connected and islanded modes) and abnormal conditions (e.g., low-voltage and low-frequency ride through, black start). With higher switching frequency and higher control bandwidth, SiC-based interface converters can have better transition between different modes and faster response for abnormal conditions.

Among other recent variations and the development of grid power converters cited earlier, SST directly benefits from the high voltage and switching capability of the HV SiC power semiconductors.

Considering the HV SiC benefits can be fully demonstrated in microgrid applications, as well as rapid growth of microgrids, the microgrid is selected to illustrate the HV SiC benefits through MV converters. The microgrid can be classified into conventional microgrid and asynchronous microgrid (i.e., with a PCS between the microgrid and distribution grid). The HV SiC benefits both in conventional and asynchronous microgrids are both investigated.

4 HV SiC benefits in conventional ac microgrids

A microgrid may contain a number of DERs, such as PV, BESS, wind energy, etc. Considering that the characteristics are similar between different kinds of DER converters, a PV system and a BESS system

are selected as representatives of DERs. The configuration of a MV conventional synchronous microgrid is shown in Fig. 14. The potential benefits of the HV SiC device-based DER converter, both at the converter level and system level, are discussed in this section.

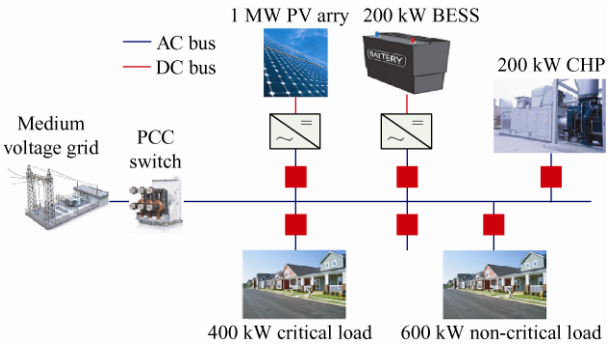

Fig. 14 Configuration of conventional synchronous microgrid

4.1 Converter-level benefits

The Si- and SiC-based utility-scale MW-class MV PV inverters are designed respectively, and compared in terms of weight, volume and efficiency. The specifications of the PV inverter are listed in Tab. 5.

Tab. 5 Specifications of PV inverter

Parameter	Value
Peak input power/MW	1.2
DC voltage, MPPT/V	600-850
Peak dc voltage/kV	1
Nominal, peak output power/MW	1, 1.2
Nominal ac voltage/kV	13.8
Grid-side current THD(%)	<5
Power factor	0.95
Efficiency(%)	>98
Grid support functions	Power curtailment, low-voltage ride through (LVRT)
Ambient temperature/℃	–40-55

4.1.1 Topology

The topology of the Si-based PV converter as shown in Fig. 15a consists of two-level voltage source inverter (600 V-850 V dc input, 400 V ac output), LCL filter, EMI filter and 400 V/13.8 kV LFT. The topology of the SiC-based PV converter as shown in Fig. 15b consists of a dc-dc converter with phase shift full bridge topology (PSFB), a three-level NPC dc-ac inverter, LCL filter, and EMI filter.

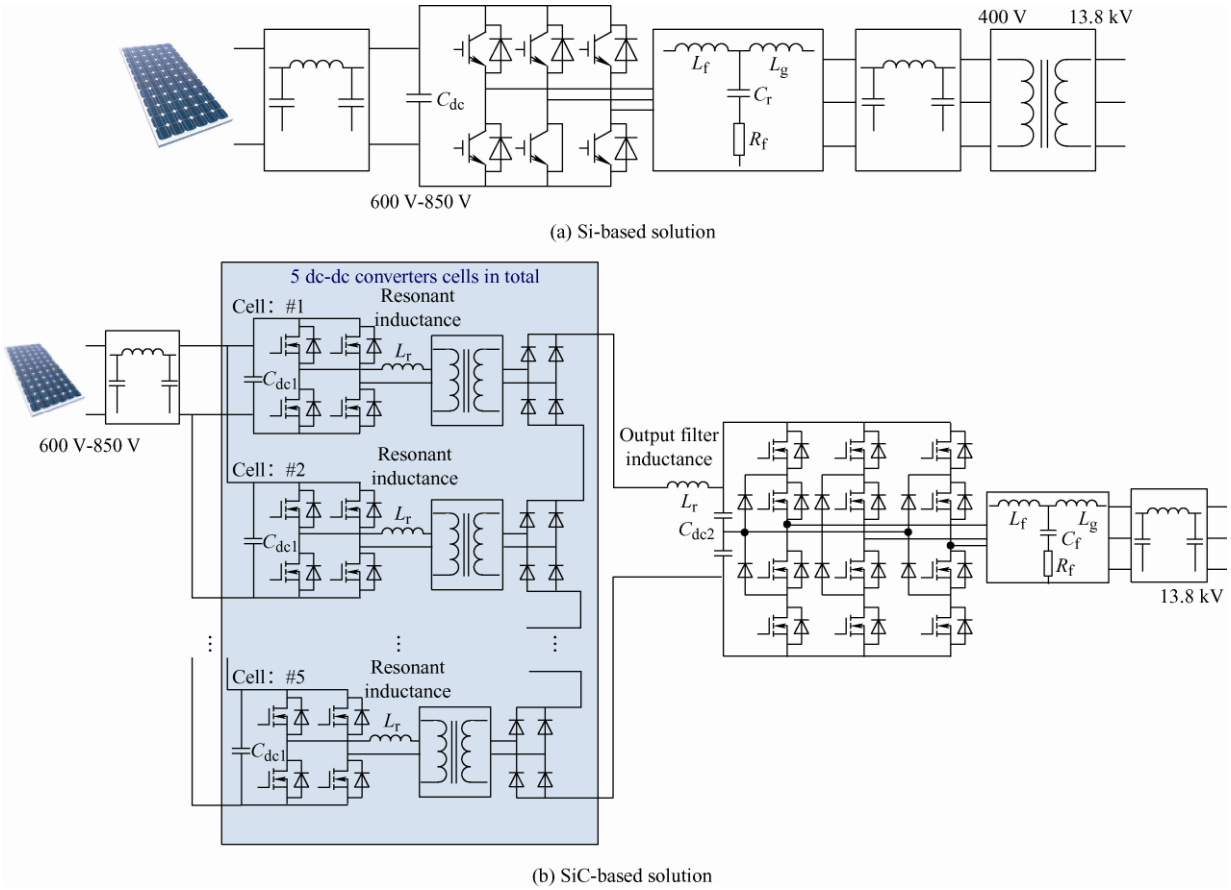

Fig. 15 Topologies of Si- and SiC-based PV inverter

4.1.2 Electrical parameter design

In order to satisfy the specifications in Tab. 5, the electrical parameters are designed based on the respective topologies in Fig. 15.

In the Si-based topology in Fig. 15a, 1.7 kV Si IGBTs are used with a control frequency of 3 kHz. The ac output voltage of the converter is 400 V and stepped up to 13.8 kV using a 60 Hz transformer. The detailed electrical parameters are described in Tab. 6.

Tab. 6 Electrical parameters of Si-based solution

Parameter	Value
DC link voltage/V	600-850
AC output voltage/V	400
Power devices	1.7 kV/6 kA Si IGBT
Control frequency/kHz	3
DC link capacitance/mF	50 (3% ΔV)
Modulation	DPWM
Filter inductor	LCL filter, 64.8 μH (0.15 p.u.)/498 μF (0.03 p.u.)/45.4 μH (0.11 p.u.)
Transformer capacity/MVA	1.2
Voltage ratio	400 V/13.8 kV
Frequency/Hz	60

In SiC-based solutions, 1.7 kV and 10 kV SiC MOSFETs are used with a control frequency of 10 kHz. The electrical parameters of SiC solution (PSFB + three-level NPC (3L NPC)) are listed in Tab. 7.

Tab. 7 Electrical parameters of SiC-based solution

Parameter	Value
PSFB dc-link voltage/V	600-850
PFSB dc capacitance/mF	15 (3% ΔV)
PFSB power devices	1.7 kV/1 kA MOSFET 10 kV/120 A diode
PFSB control frequency/kHz	10
PFSB output inductance/mH	42
3L NPC dc-link voltage/kV	21
3L NPC ac output voltage/kV	13.8
3L NPC dc capacitance/μF	28(3% ΔV)
3L NPC power devices	15 kV/160 A MOSFET
3L NPC control frequency/kHz	10
3L NPC modulation	SVPWM
3L NPC filter inductor	LCL filter, 15.6 mH (0.03 p.u.)/ 190 nF (0.015 p.u.)/ 11.7 mH (0.023 p.u.)

4.1.3 Physical design comparison

The component physical design in Si and SiC solutions can be completed according to the electrical parameters, including heatsink, passives, etc. The comparison of the weights and volumes are shown in Fig. 16. The power losses of Si- and SiC-based PV inverters are nearly the same (15.7 kW in SiC-based and 16.2 kW in Si-based) per efficiency requirement, as shown in Fig. 17. However, the weight and size of the SiC-based PV inverter are reduced by 82.9% and 73.2% compared to those of the Si-based converter. Most of the savings come from the transformer and the filter inductor. Consequently, the power density of the SiC-based inverter is 3.75 times that of the Si-based converter (0.81 MW/m^3 for the SiC-based and 0.216 MW/m^3 for Si-based) and the specific power of the SiC-based converter is 5.87 times that of the Si-based converter (1.11 MW/ton for the SiC-based and 0.189 MW/ton for Si-based).

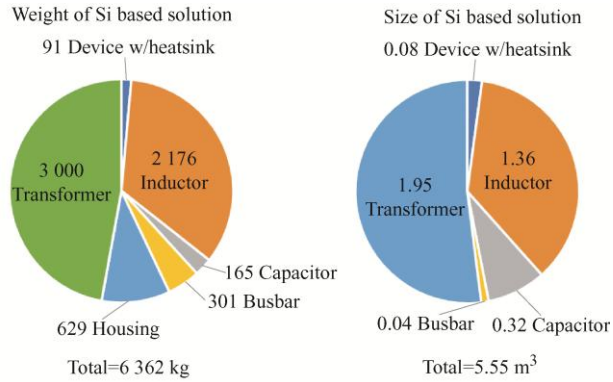

(a) Weight and volume of Si-based solution

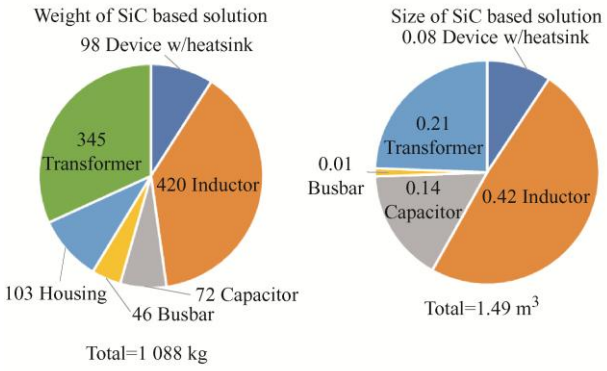

(b) Weight and volume of SiC-based solution

Fig. 16 Weight and volume comparison between Si- and SiC-based solutions

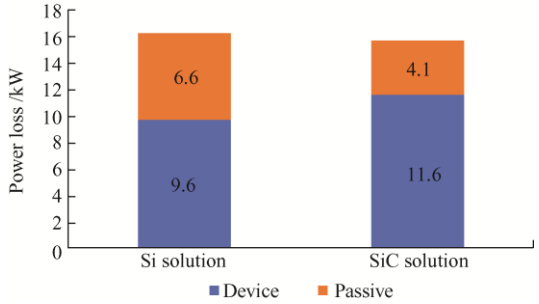

Fig. 17 Power loss comparison of Si and SiC solutions

4.2 System-level benefits

As mentioned above, the control frequency of SiC-based converter can be 10 times higher than the Si-based. Therefore, the control bandwidth of the SiC-based converter can be significantly increased, bringing benefits in system-level such as power-quality improvement, system stability enhancement and low-voltage ride through (LVRT) [55-57].

4.2.1 Power quality improvement

The growing use of electronic equipment can result in significant harmonics in power-distribution systems due to non-sinusoidal currents consumed by non-linear loads. Some of the examples for non-linear loads are diode or thyristor rectifiers used for heating-ventilation-air conditioning and adjustable speed drives, furnaces, computer/data center power supplies, uninterruptible power supplies, etc. Even though these devices are economical, flexible, and energy efficient, they may degrade power quality by generating harmonic currents and voltages.

Harmonic distortion in power distribution systems can be suppressed using two approaches, namely, passive and active power filtering [55]. Passive filters using inductors and capacitors have drawbacks, such as bulky size, possibility of resonance, and fixed inflexible compensation. Since SiC-based converter can provide active filtering function, only active filtering is studied here.

For the Si-based solution, a dedicated Si-based APF with high switching frequency is needed. For the SiC-based solution, thanks to the high switching frequency capability and corresponding high control bandwidth of SiC-based converters, the filtering function can be integrated into DER interface converters themselves, and therefore no additional APF is required. The setup for comparing the two solutions is shown in Fig. 18. In this case, the SiC-based PV interface converter is used for harmonic compensation. The target is to maintain the total demand distortion (TDD) of the point of common coupling (PCC) on the grid side below 5%.

The TDD simulation results are shown in Fig. 19. Without harmonic compensation, 14.0% harmonic current, which is from the non-linear six-pulse uncontrolled rectifier load, is injected into the grid. TDD becomes less than 5% both with Si-based and SiC-based solution. However, the 150 kVA additional APF can be saved in the SiC-based solution.

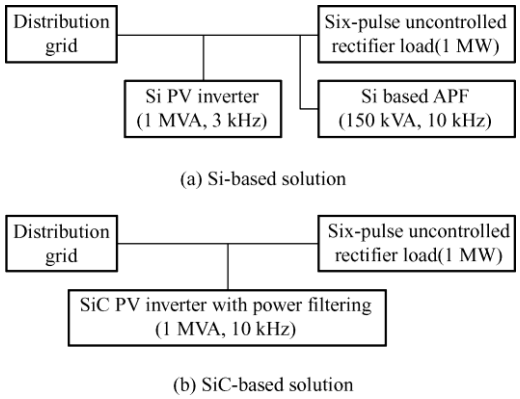

Fig. 18 Setup of comparison for Si and SiC solutions

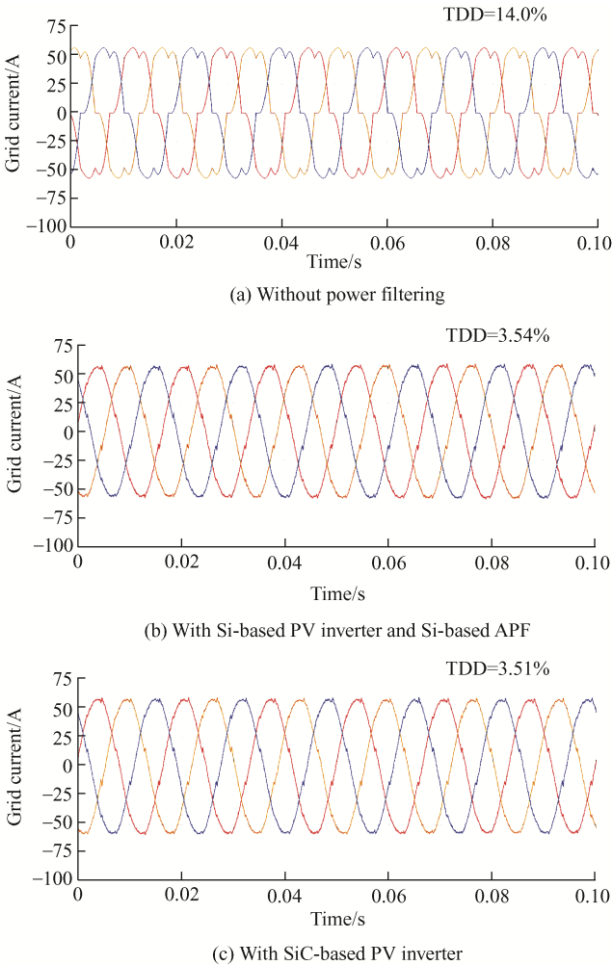

Fig. 19 Grid current with Si- and SiC-based solutions

4.2.2 System stability enhancement

Multiple renewable energy and energy-storage interface converters in microgrids, connected to relatively weak grids, can lead to harmonic resonance and stability issues. SiC-based converters, with their

switching frequency and high control bandwidth, can help damp the resonance and enhance stability.

The impedance-based stability criteria are effective in analyzing the small-signal stability of systems consisting of power electronics converters [56]. The interconnected system is stable if and only if the impedance ratio at the interconnection interface meets the Nyquist stability criterion. A conservative derivative of the Nyquist stability criterion is the passivity-based stability criterion, that is, the overall system stability is guaranteed if the impedance phase angle of each individual subsystem is within [−90° , 90°]. For example, for three-phase converters with LCL filters and grid-side current control, the non-passive frequency range, where the phase angle of the converter output admittance is outside of [−90° , 90°], is between the resonance frequency ω_r of the converter-side inductor L_f and the filter capacitor C_f as expressed in Eq. (1), and the critical frequency ω_d determined by the delay time T_d in the converter control loop as expressed in Eq. (2), where T_d is 1.5 times the switching period (T_s). According to the passivity-based stability criterion, the negative conductance of converters could trigger unstable resonance in the system.

$$\omega_r = \frac{1}{\sqrt{L_f C_f}} \tag{1}$$

$$\omega_d = \frac{\pi}{2T_d} = \frac{\pi}{3T_s} \tag{2}$$

Considering the switching frequency of SiC-based converter is much higher than Si, the non-passive frequency range of SiC-based converter can get rid of the resonance frequency caused by the weak grid, thus enhance the grid stability. The typical open-loop gains of Si- and SiC-based converters are shown in Fig. 20.

When connecting the DER interface converters to a weak grid, a potential resonance circuit is formed by the large grid inductor L_s and parasitic capacitors along the cable or the power factor correction (PFC) capacitors installed at the PCC, denoted as C_p, and the potential resonance frequency ω_{rg} is expressed in Eq. (3). For a weaker grid with a larger grid inductance L_s, the resonance frequency ω_{rg} is lower.

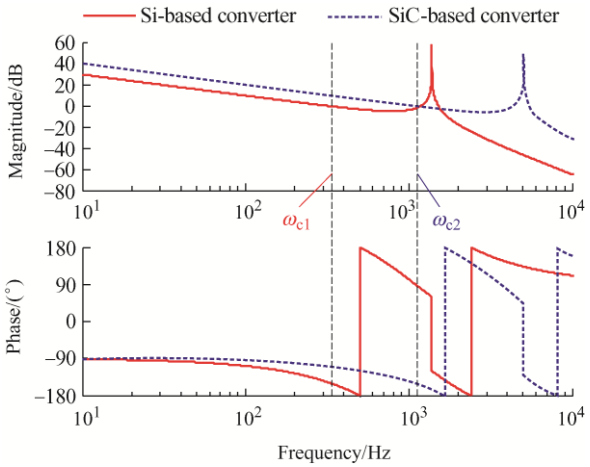

Fig. 20 Bode plots of the current open-loop gains of the Si-based converter and the SiC-based converter

$$\omega_{rg} = \frac{1}{\sqrt{L_s C_p}} \tag{3}$$

Thanks to the advantages of a higher switching frequency and a smaller time delay in the control loop, the SiC-based converter possesses a non-passive range in the higher frequency range, compared with that of the Si-based converter. Therefore, when connected to a weak grid, the SiC-based converter has a smaller destabilization effect on the system stability, compared with the Si-based converter. In other words, weak grids with SiC-based converters have better stability than those with Si-based converters.

Several simulations are carried out to verify the benefit of system stability enhancement brought by the SiC-based converters. In the following simulations, two grid conditions are considered, as shown in Fig. 21: a normal grid with impedance of 0.05 p.u. and a weak grid with impedance of 0.1 p.u.; The PFC grid capacitor is assumed as 0.044 p.u.; For the DER interface converter, two cases are compared including Si-based (M1) and SiC-based DER converters (M2).

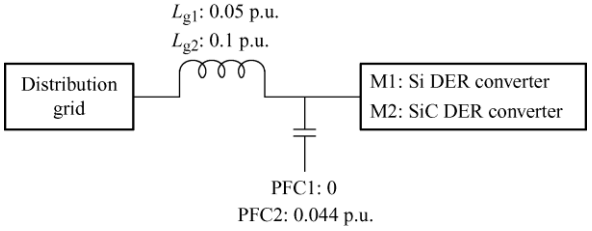

Fig. 21 Setup of stability investigation

With M1, the simulation results are shown in Fig. 22. The grid is stable in the normal grid (L_g=0.05 p.u., PFC=0), however, becomes unstable in the weak

grid with the PFC capacitor (L_g=0.1 p.u., PFC=0.044 p.u.). However, with M2, the grid is stable in both conditions, as shown in Fig. 23.

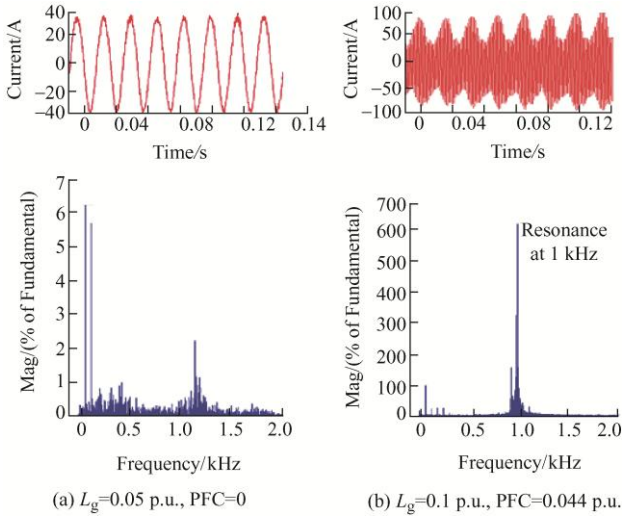

Fig. 22 FFT analysis of grid current with Si DER converter

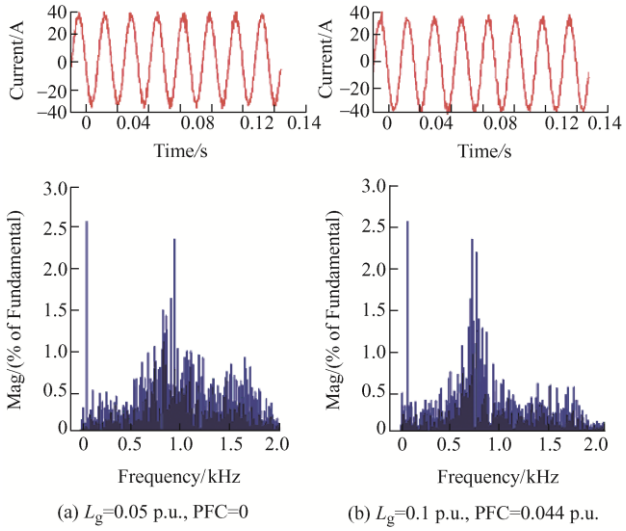

Fig. 23 FFT analysis of grid current with SiC DER converter

4.2.3 Low-voltage ride through

In power systems, LVRT is the capability of electric generation to stay connected for short periods of lower electric network voltage [57]. It is needed at the distribution level (wind farms, PV systems, BESSs, distributed cogeneration, etc.) to avoid that a short circuit fault leads to a widespread loss of generation. The detailed performance requirements of LVRT for DER are presented in IEEE Std 1547-2018, as shown in Fig. 24.

The simulation results of LVRT are show in Fig. 25. The operation steps during LVRT period are as follows. (1) DER system supplies rated active power and zero reactive power (I_d=1 p.u., I_q=0) until the PCC voltage drop occurs (0.2 s). (2) A PCC voltage drop (45% of base voltage) is detected. The DER system begins to supply zero active power and rated reactive power (I_d=0, I_q=1 p.u.). (3) After 160 ms, the PCC voltage returns to the rated voltage. The DER system recovers to normal operation. The LVRT can be achieved with either Si-based interface converter or SiC-based one. However, due to the higher control bandwidth, the dynamic performance with SiC-based converter is better (lower grid and converter peak current and shorter response time).

Interconnection system default response to abnormal voltages

Default settings[a]		
Voltage range (% of base voltage[b])	Clearing time /s	Clearing time: Adjustable up to and including/s
V<45	0.16	0.16
45≤V<60	1	11
60≤V<88	2	21
110<V<120	1	13
V≥120	0.16	0.16

[a] Under mutual agreement between the EPS and DR operators, other static or dynamic voltage and clearing time trip settings shall be permitted
[b] Base voltages are the nominal system voltages stated in ANSI C84.1-2011,Table 1.

Fig. 24 LVRT requirement in IEEE Std 1547-2018

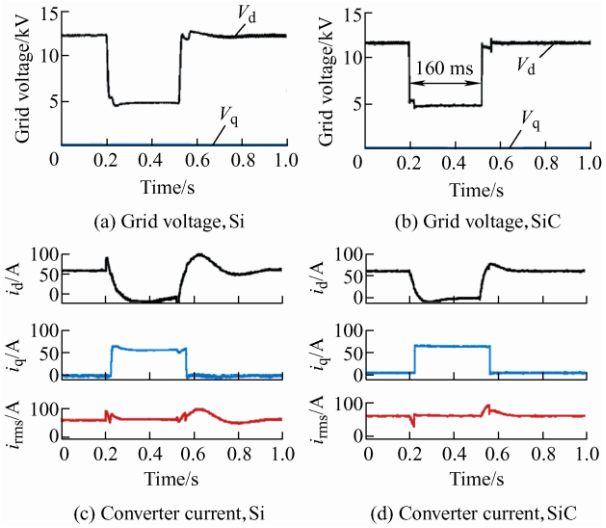

Fig. 25 LVRT comparison of Si and SiC DER converter

5 Benefits of HV SiC-based asynchronous microgrid PCS

A PCS for asynchronous microgrid is used as an example to investigate the benefits by comparing Si- and SiC-based solutions. The asynchronous microgrid concept is shown in Fig. 26; the asynchronous microgrid PCS is an ac-ac converter, which consists of an ac-dc converter (on the grid side) and a dc-ac converter (on the microgrid side), working as the interface between the ac microgrid and the distribution grid. The specifications of the PCS are listed in Tab. 8. The comparison can be extended to other power

converters in distribution grids.

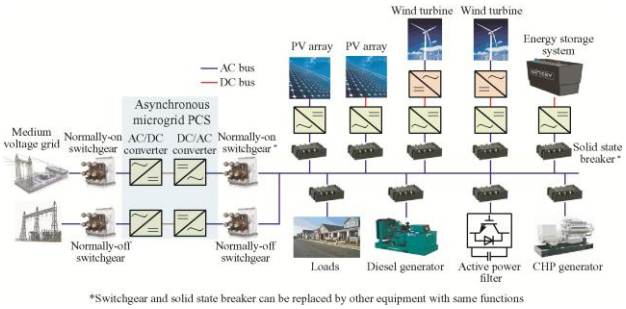

Fig. 26 Asynchronous microgrid with PCS

Tab. 8 Specifications of PCS

Parameter	Value
Power rating/MVA	1
Nominal ac voltage/kV	13.8
Grid-side current THD(%)	<5
Efficiency(%)	>98
Grid support functions	Low/high-voltage/frequency ride through, grid-connected/islanded operation, active power filtering, etc.
Ambient temperature/℃	–40-55

5.1 Converter-level benefits

In order to investigate the converter-level benefits, the Si-based and SiC-based PCS are designed respectively, and compared in terms of weight, volume and efficiency.

5.1.1 Topology

For the Si-based solution, a commercial PCS, using three-level NPC converter based on HV Si IGBTs and step-up transformers, is selected as a baseline for comparison. The topology is shown in Fig. 27a. The step-up LFT can be eliminated in SiC-based PCS, considering voltage ratings of SiC power semiconductors are higher than Si. The five-level NPC and modular multilevel converter (MMC) topologies are selected for SiC-based solutions, as shown in Fig. 27b and Fig. 27c.

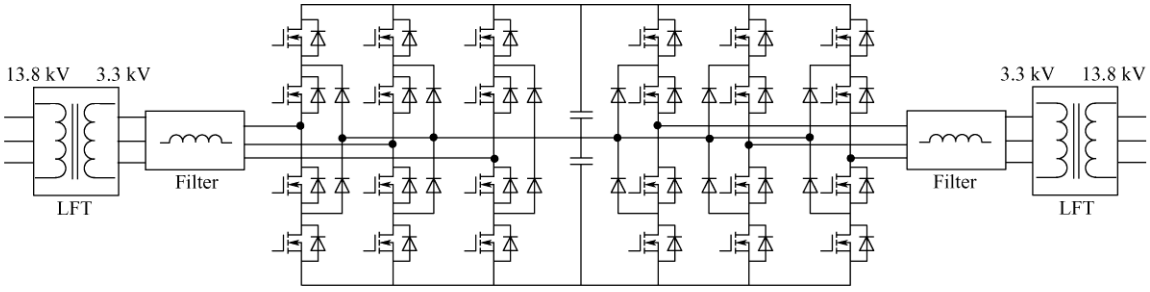

(a) Si-based solution, three-level NPC + step-up transformer

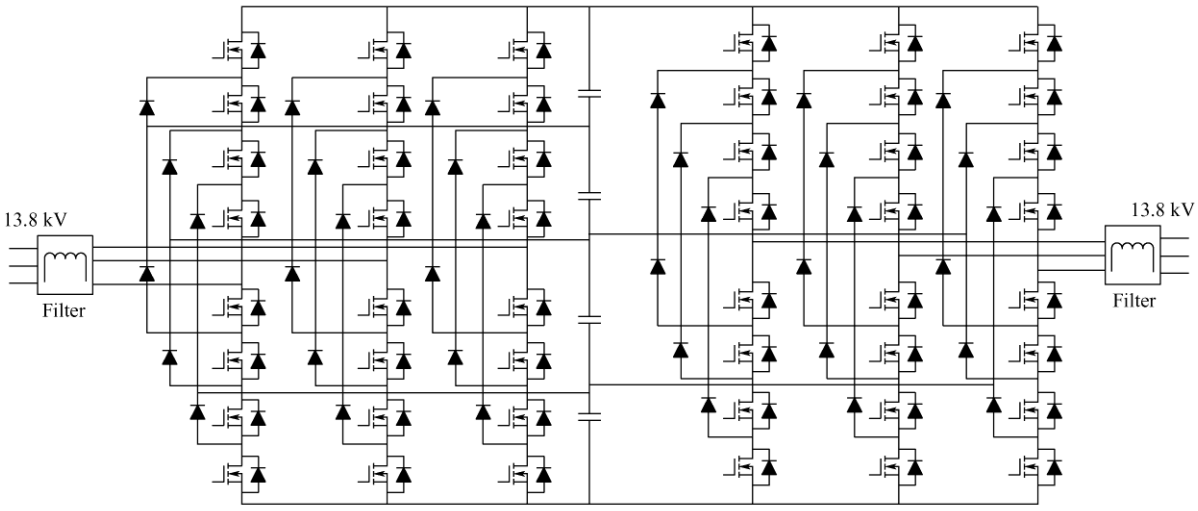

(b) SiC-based solution 1(S1), five-level NPC

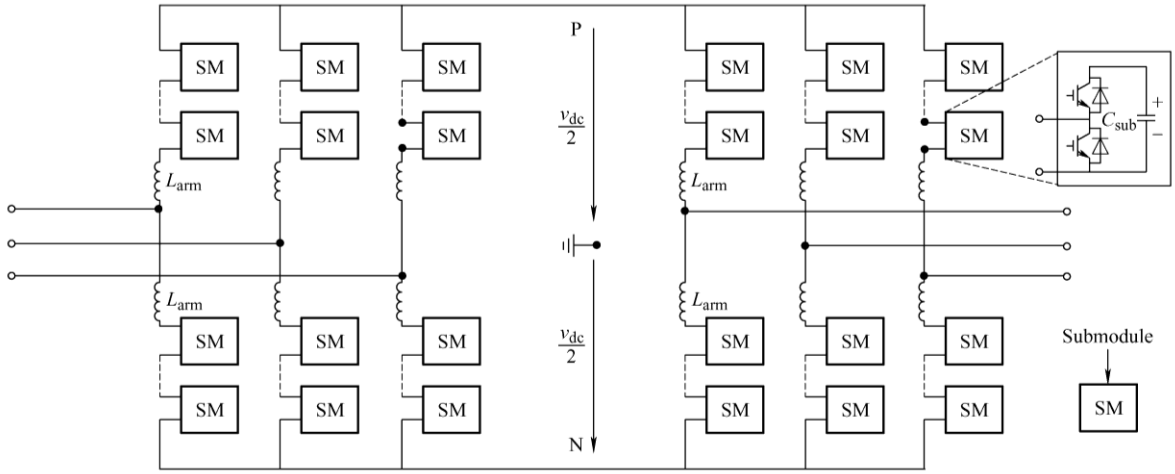

(c) SiC-based solution 2(S2), five-level MMC

Fig. 27 Topologies of Si- and SiC-based PCS

5.1.2 Electrical parameter design

In order to satisfy the specifications in Tab. 8, the electrical parameters are designed based on three topologies in Fig. 27, respectively.

In the Si-based topology in Fig. 27a, 4.5 kV Si IGBTs are used with a control frequency of 1 kHz. The ac output voltage of the converter is 3.3 kV and stepped up to 13.8 kV using a 60 Hz transformer. The detailed electrical parameters are described in Tab. 9.

Tab. 9 Electrical parameters of Si-based solution

Parameter	Value
DC link voltage/kV	5.3
AC output voltage/kV	3.3
Power devices	4.5 kV/600 A Si IGBT
Control frequency/kHz	1
DC link capacitance/mF	2.4(3% ΔV)
Modulation	SVPWM
Filter inductor/mH	7.2(0.25 p.u.)
Transformer capacity/MVA	1.1
Voltage ratio	3.3 kV/13.8 kV
Frequency/Hz	60

In SiC-based solutions, 10 kV SiC MOSFETs are used with a control frequency of 20 kHz. The electrical parameters of SiC-based solution 1(S1, five-level NPC) are listed in Tab. 10.

Tab. 10 Electrical parameters of SiC S1 (five-level NPC)

Parameter	Value
DC link voltage/kV	25
AC output voltage/kV	13.8
Power devices	10 kV/150 A SiC MOSFET
Control frequency/kHz	20
DC link capacitance/μF	6(3% ΔV)
Modulation	SPWM without 3rd harmonic injection
Filter inductor/mH	5.2 (0.01 p.u.)

A submodule (SM) is a basic unit in SiC-based MMC, which is also designed based on a 10 kV SiC MOSFET with a control frequency of 15 kHz. The electrical parameters of SiC-based solution 2 (S2, five-level MMC) are listed in Tab. 11.

Tab. 11 Electrical parameters of SiC S2 (five-level MMC)

Parameter	Value
DC link voltage/kV	25
AC output voltage/kV	13.8
Power devices	10 kV/100 A SiC MOSFET
Control frequency/kHz	15
SM number per arm	4
SM voltage/kV	6.25
SM capacitance/μF	66
Arm inductance/mH	6.7(0.013 p.u.)
Line inductance/mH	1(0.002 p.u.)

5.1.3 Physical design comparison

According to electrical parameters, the component physical design in the above three solutions (i.e., Si-based solution, and SiC-based NPC and MMC) can be completed, including heatsink, passives, etc. A comparison of the weight and volume is shown in Fig. 28. Because there is no need for bulky LFT and because passive inductors and capacitors are smaller, SiC-based PCS can significantly reduce the weight and volume (e.g., 94% reduction in weight for NPC and 85% for MMC, and 91% reduction in volume for NPC and 83% for MMC). In terms of efficiency, the efficiency of

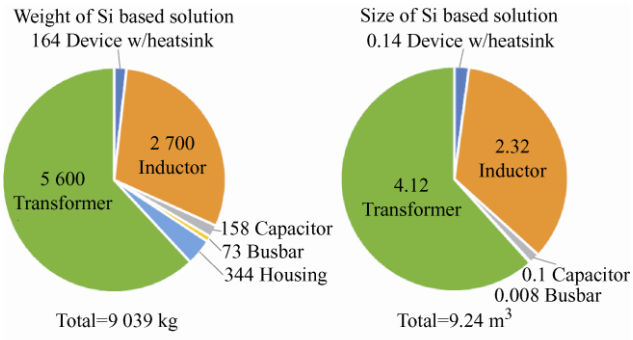

(a) Weight and volume of Si-based solution

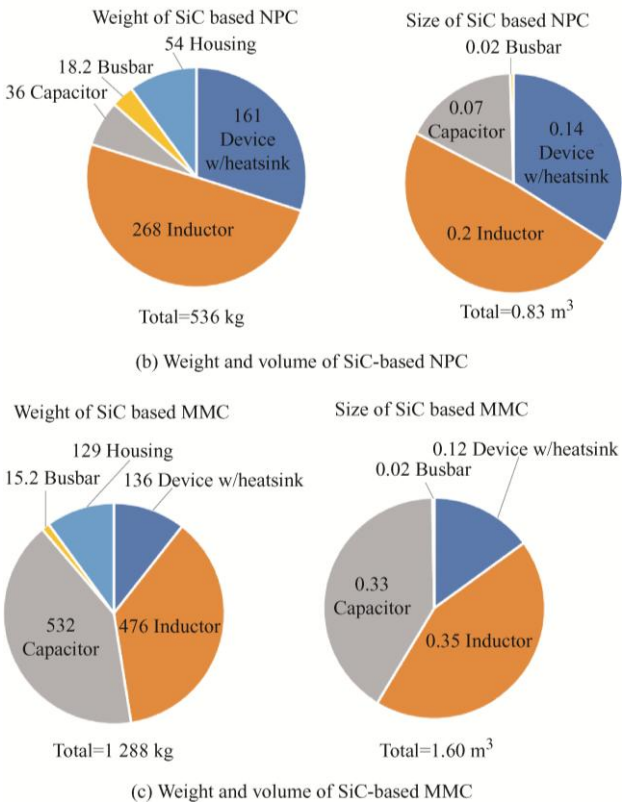

Fig. 28 Weight and volume comparison between Si- and SiC-based solutions

Si-based PCS can reach 98.52% with a control frequency of 1 kHz and without considering the power loss of the LFT, while the estimated efficiencies of SiC-based solutions are 98.57% with a control frequency of 20 kHz for NPC and 98.64% with control frequency of 15 kHz for MMC, as shown in Fig. 29. Even though the control frequency is considerably increased for SiC-based solutions, the efficiencies of the Si- and SiC-based solutions are similar. If the power loss of the transformer is considered (e.g., 99% for the transformer), the efficiency of SiC PCS is higher than that of Si PCS.

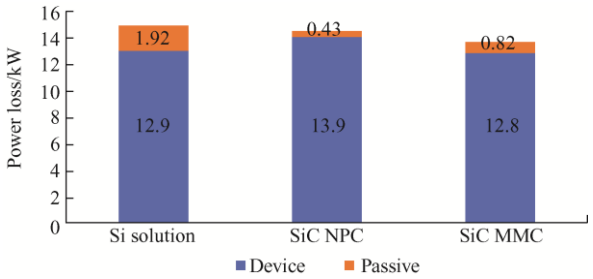

Fig. 29 Power loss comparison of Si and SiC solutions

5.2 System-level benefits

The potential system-level benefits of asynchronous microgrids with PCS as well as SiC-based PCS are summarized in Tab. 12. The asynchronous microgrid can lead to many system-level benefits. However, not all of these benefits can utilize the fast switching capabilities enabled by SiC. This section focuses on the system-level issues that can potentially benefit from SiC solutions, including power quality, stability, LVRT, transition between grid-connected mode and islanded mode, and black start [55-59].

Tab. 12 Potential system-level benefits of the SiC-based microgrid PCS

Use case	Benefits of microgrid PCS	Benefits of SiC PCS
	Grid-connected mode	
Frequency & voltage control	Easy for (a) reactive power support, for both sides independently; and (b) power transfer control	Not obvious (smaller filter for more var), dynamic response
Stability	Isolation—Can isolate stability issue of microgrid, enabling easy integration of high renewable microgrid with the existing ac grid. small-signal stability—Generally simplifies the design for stability. A microgrid stable in the islanded case can be more easily integrated with the ac grid. Oscillation damping & voltage stability—Easier inertia emulation & var support	small-signal stability-faster SiC can help control and impedance forming Oscillation damping faster SiC can help with inertia emulation & var support
Power quality	Interface converters can provide APF functions for both ac grid and microgrid. Can save dedicated filters	APF function only effective with SiC
LVRT	No voltage drop in microgrid, load voltage maintained	Better dynamic response
Multi-feeder microgrid	Easy to achieve microgrid with multiple feeders: (a) no need for information on voltage amplitude and phase of feeders, and (b) easy to isolate from the faulted feeder, and maintain the connection with other feeders; easy power flow	Not obvious
Short circuit current	Short circuit current is reduced with the asynchronous microgrid, as the interface converters isolate/limit fault-current contributions	Not obvious
Efficiency	Incurs additional loss during normal operation—A drawback of the microgrid PCS	SiC can have lower power loss than Si
	Islanded mode	
Transition	Seamless transition between grid-connected and islanded modes, no voltage drop in microgrid	Better dynamic response
Frequency & voltage control	Microgrid side PCS provides var support	Not obvious
Stability	Microgrid PCS could be a stabilizer	Faster SiC can help control and form impedance
Power quality	Microgrid side interface converter can provide APF function when SiC is applied for MG, reducing or eliminating the need for dedicated filters	APF function only effective with SiC
Black start	Black start is easy with Microgrid PCS, but there is no obvious benefit over traditional islanded microgrid	Not obvious

5.2.1 Power quality improvement

Similar to the case in the conventional microgrid, for the Si-based solution, a dedicated Si-based APF with high switching frequency is needed; for the SiC-based solution, the filtering function can be integrated into the PCS. The setup for comparing the two solutions is shown in Fig. 30.

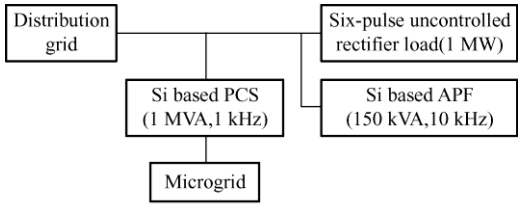

(a) Si-based solution

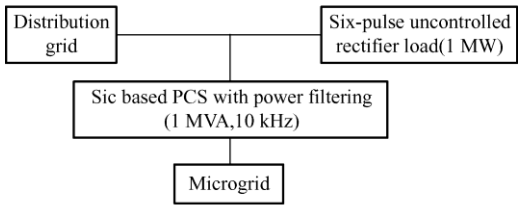

(b) SiC-based solution

Fig. 30 Setup of comparison for Si and SiC solutions

The simulation results are shown in Fig. 31, indicating that Si and SiC solutions can both meet the <5% TDD requirement. However, for the Si-based solution, the converter rating is the sum of converter ratings of the Si-based PCS and the Si-based APF (i.e., an additional 150 kVA APF is required, resulting in a total converter rating of 1.15 MVA). However, in SiC solution, the APF can be saved and the total converter rating is only slightly (about 1%) over 1 MVA.

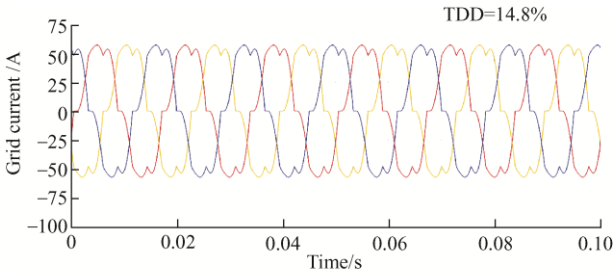

(a) without power filtering

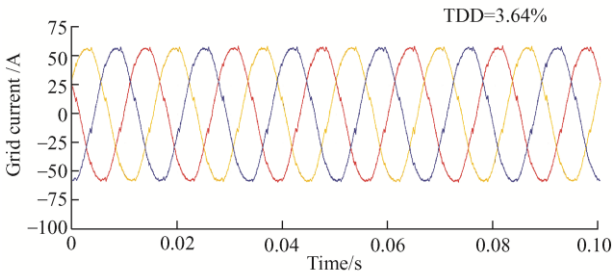

(b) With Si-based PCS and Si-based APF

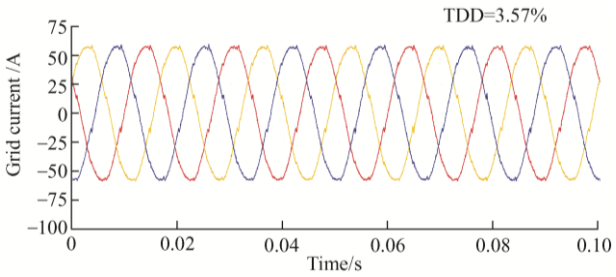

(c) With SiC-based PCS

Fig. 31 Grid current with Si-based and SiC-based solutions

5.2.2 System stability enhancement

SiC-based PCS can bring benefits on the stability of the asynchronous microgrid in both grid-connected mode and the islanded mode.

(1) Grid-connected mode

Different cases with various grid impedances, as shown in Fig. 32, are investigated in order for stability analysis in grid-connected mode. On the grid side, the grid impedances are selected as 0.05 p.u. (normal grid) and 0.1 p.u. (relatively weak grid). The PFC capacitances are selected as 0 (without PFC capacitor) and 0.163 p.u. (with PFC capacitor). In terms of the microgrid, three cases are compared including microgrid without PCS (M1), microgrid with Si-based PCS (M2), microgrid with SiC-based PCS (M3).

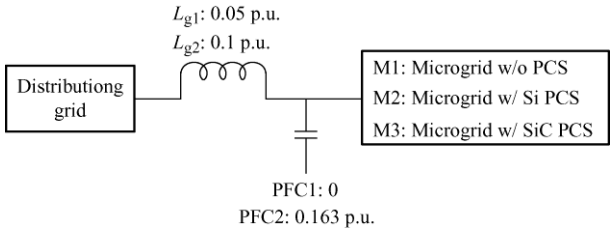

Fig. 32 Setup of stability investigation

With M1, considering the complex impedance of the microgrid (e.g., multiple DER interface converters within the microgrid), the grid is stable with a normal grid impedance (L_g=0.05 p.u.), however, becomes unstable in a weak grid condition (L_g=0.1 p.u.), as shown in Fig. 33a. With M2, the microgrid impedance can be isolated by the PCS, and the grid stability can be maintained even in weak grid condition (L_g=0.1 p.u.), as shown in Fig. 33b. However, if the PFC capacitor is placed (PFC=0.163 p.u.), the grid becomes unstable again, as shown in Fig. 33c. With M3, the

grid is stable even with the weak grid condition (L_g=0.1 p.u.) and PFC capacitor (PFC=0.163 p.u.), as shown in Fig. 33d. It can be concluded that with SiC-based PCS, the grid stability is better than that of without PCS and with Si-based PCS (i.e., the stability can be maintained under various grid impedance values).

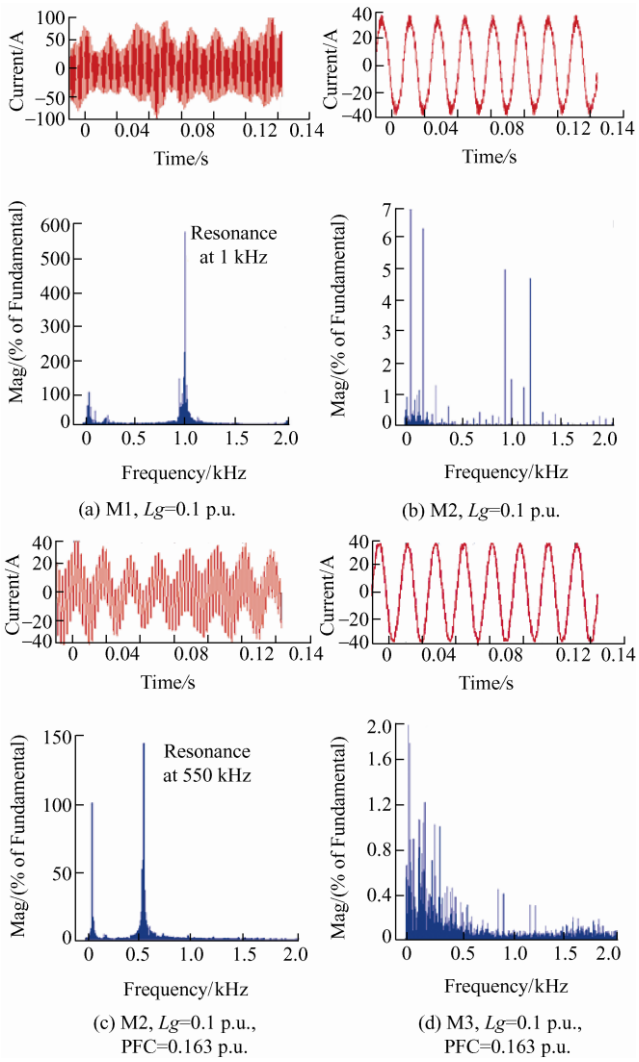

Fig. 33 FFT analysis of grid current in grid-connected mode

(2) Islanded mode

Within the microgrid, because of multiple DER interface converters in parallel, the stability issue is a significant challenge for microgrid design. Similar to the case of the grid-connected mode, in the islanded mode, the SiC-based PCS can also enhance the stability within the microgrid due to its high switching frequency and control bandwidth. Simulation results of Si- and SiC-based PCS are compared in Fig. 34. In the simulated scenario of the microgrid, there are 2 PV inverters and 2 battery storage systems. It can be seen that with SiC-based PCS, the microgrid stability is also improved.

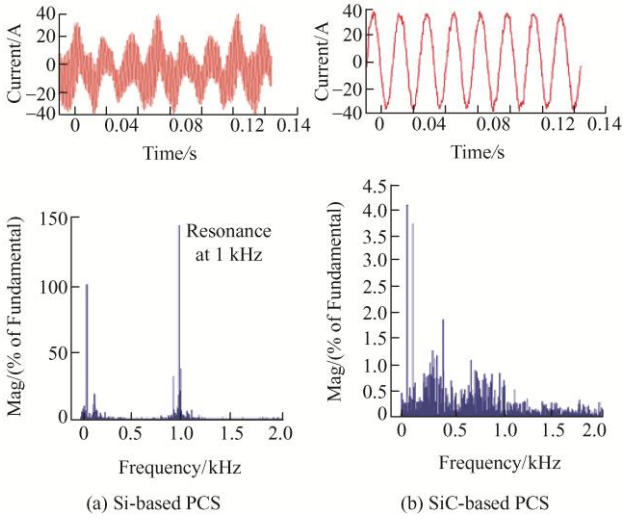

Fig. 34 FFT analysis of microgrid current in islanded mode

5.2.3 Low-voltage ride through

In the conventional ac microgrid, the DER converters have LVRT capability. However, due to the voltage drop at PCC, loads have to operate abnormally. By using the asynchronous microgrid PCS, there is no voltage drop at PCC of microgrid side and the load voltage is maintained. The LVRT performance using Si- and SiC-based PCS is simulated in this subsection.

The simulation results are shown in Fig. 35. The operation steps during LVRT period are as follows. (1) The grid supplies the power to the load until the grid voltage drop starts (0.1 s). (2) A grid voltage drop (45% of the rated voltage) is detected. The microgrid PCS converter on the grid-side VSC1 operates in LVRT mode and supplies 1.0 p.u. reactive current. The converter on the microgrid side VSC2 transitions to rectifier mode such that the dc-link voltage of microgrid PCS can be maintained. (3) After 160 ms, the grid voltage returns to the rated voltage. The microgrid recovers to the operation prior to Step 1. The PCC voltage on the microgrid side, which is also the load voltage, can be maintained both with Si- and SiC-based microgrid PCS. However, due to the higher control bandwidth, the dynamic performance with SiC-based converter is better (lower peak current and shorter response time).

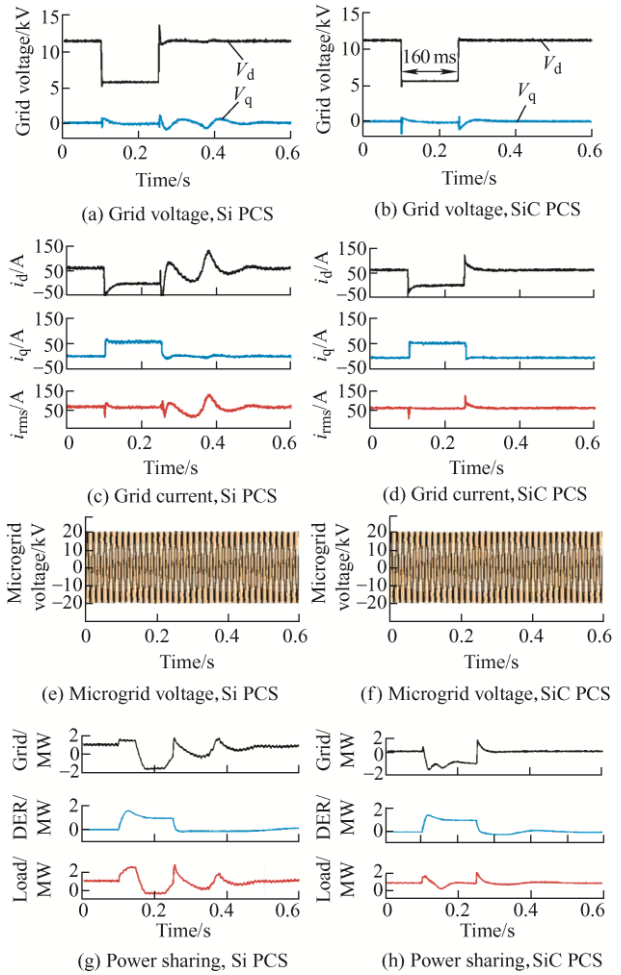

(a) Grid voltage, Si PCS (b) Grid voltage, SiC PCS
(c) Grid current, Si PCS (d) Grid current, SiC PCS
(e) Microgrid voltage, Si PCS (f) Microgrid voltage, SiC PCS
(g) Power sharing, Si PCS (h) Power sharing, SiC PCS

Fig. 35 LVRT comparison of Si- and SiC-based PCS

5.2.4 Mode transition

The transition between the islanded mode and grid-connected mode is evaluated in this section [58]. Sometimes the transition occurs on purpose (i.e., intentional islanding) but in most cases, the transition takes place when a grid fault occurs, such as the grid voltage drop as a result of short-circuit fault. With a conventional ac microgrid, when a grid voltage drop is detected, the DER interface converter attempts LVRT first based on the IEEE Std 1547-2018. After the LVRT period, the microgrid can be disconnected and operates in islanded mode if the fault is not cleared. There is one obvious drawback with the conventional ac microgrid during mode transition, the load operates abnormally due to the voltage drop during the LVRT period. In asynchronous microgrid with PCS, during the transition period, the microgrid is isolated from the grid and the load voltage can be maintained. The simulation results of mode transition are compared between Si- and SiC-based PCS.

The simulation results are shown in Fig. 36. The operation steps with the PCS during transition period are, as follows. (1) Operation in grid-connected mode until the grid voltage starts to drop (0.1 s). (2) A grid voltage drop (45% of rated voltage) is detected. The microgrid PCS converter on the grid side VSC1 transitions from rectifier mode to LVRT mode and supplies 1.0 p.u. reactive current. The converter on the microgrid side VSC2 transitions from droop control to rectifier mode such that the dc-link voltage of microgrid PCS can be maintained. (3) After 160 ms, if the grid voltage is not recovered, VSC1 is shut down and the microgrid is disconnected. Without the PCS, all the DER interface converters in microgrid have to transition from droop control to LVRT mode and the load withstands the low voltage in Step 2. With the PCS, a seamless transition between grid-connected mode and islanded mode can be achieved. The PCC voltage in the microgrid can be maintained and the load is supplied normally. The dynamic performance with SiC-based PCS is better than Si-based counterpart due to the high control bandwidth.

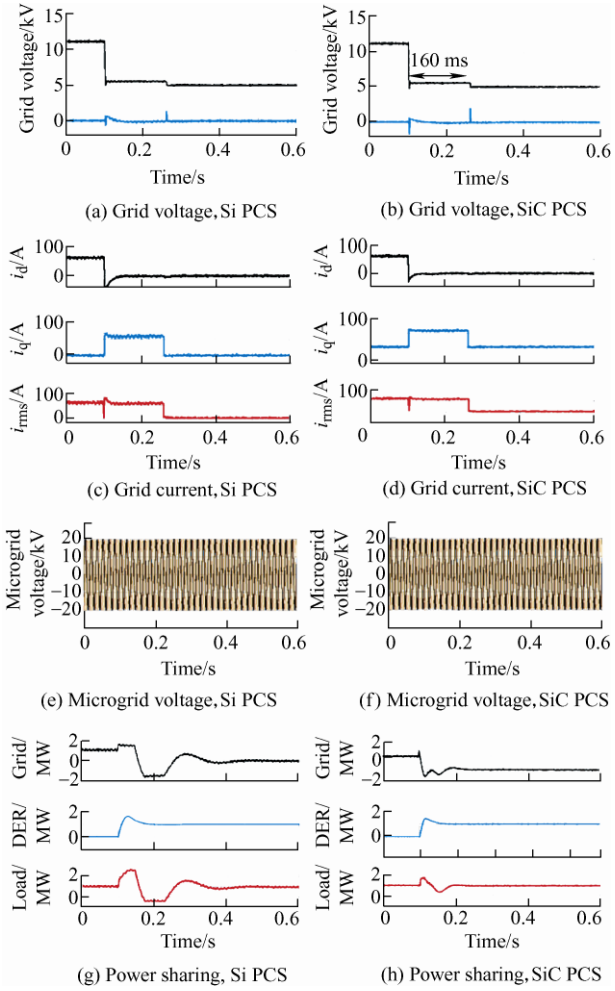

(a) Grid voltage, Si PCS (b) Grid voltage, SiC PCS
(c) Grid current, Si PCS (d) Grid current, SiC PCS
(e) Microgrid voltage, Si PCS (f) Microgrid voltage, SiC PCS
(g) Power sharing, Si PCS (h) Power sharing, SiC PCS

Fig. 36 Mode transition comparison of Si- and SiC-based PCS

5.2.5 Black start

The black start is the procedure of restoring an electric power station or a part of an electric grid to operation without relying on external network [59]. With or without the asynchronous microgrid PCS, the microgrid is required to have black start capability based on IEEE Std 2030.7. First, the microgrid should perform black start internally during islanded operation for local service restoration. Then the microgrid can reconnect to the utility distribution grid.

The simulation results of black start with and without the PCS are show in Fig. 37. The black start steps with microgrid PCS are as follows. (1) Build up the PCC voltage in the microgrid by BESS (0.1 s). The PCS dc-link voltage is established by microgrid side converter VSC2. (2) PV system is put into operation and the load in the microgrid is powered (0.3 s). (3) Synchronize (from 0.2 s to 0.45 s) with the grid using grid side PCS converter VSC1. (4) Transition to grid-connected mode (0.5 s). The black start with microgrid PCS is easier because the resynchronization can be completed only with VSC1. The dynamic performance with SiC-based MG PCS is better than Si-based due to the higher control bandwidth.

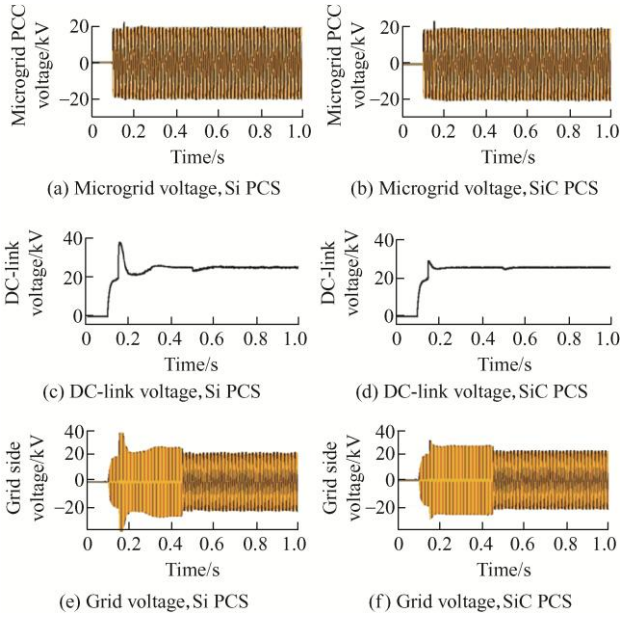

Fig. 37 Black start comparison of Si- and SiC-based PCS

6 HV SiC-based PCS development

A 13.8 kV/100 kVA asynchronous microgrid PCS prototype using 10 kV SiC MOSFET has been developed as shown in Fig. 38, supported by Power America Program. The issues related to HV SiC device utilization have been addressed during the project, including device characterization and modeling [60], gate driver [61], isolated power supply [62], sensor [63], passive, thermal management [64], modulation [65], control [66], and testing [67].

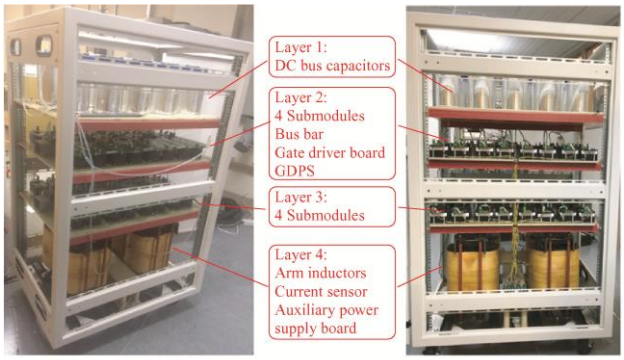

Fig. 38 Asynchronous microgrid PCS prototype

The estimated efficiency at a 10 kHz control frequency is 98.6%. The specific power and power density of the developed PCS are 0.14 kW/kg and 80 kW/m^3, respectively. The arm inductor is a major contributor to the weight and size. Without the inductor, the specific power and power density could reach 1.17 kW/kg and 240 kW/m^3, respectively. Furthermore, the high-voltage insulation material accounts for a large percentage of the power converter volume, which does not scale proportionally with increasing power. Therefore, the specific power and power density of the converter improve for higher power ratings (e.g., 1 MW).

Fig. 39 shows the phase-leg test waveforms including a) PWM output voltage at 12 kV dc-link and b) ac output voltage at 25 kV dc-link, demonstrating the normal operation for the developed 10 kV SiC MOSFET-based PCS converter. The high-voltage probe suffers from partial discharge issue to measure the PWM output voltage at a dc-link voltage higher than 12 kV. Therefore, at 25 kV dc-link (i.e., nominal dc-link), only the ac output voltage is tested.

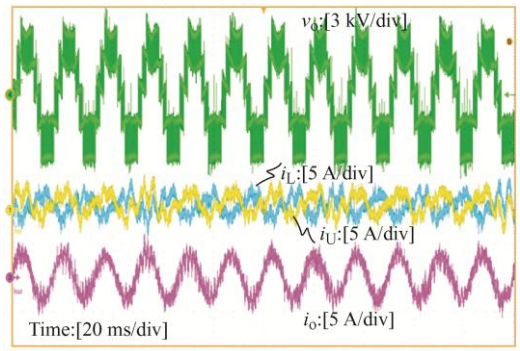

(a) PWM output at 12 kV dc-link

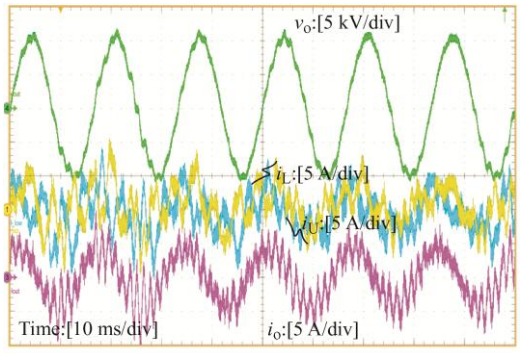

(b) ac output at 25 kV dc-link

Fig. 39 PCS waveforms at 12 kV and 25 kV dc-link

7 Conclusions

Compared to conventional Si devices, SiC devices have advantages in voltage rating, switching frequency, etc. The latest HV SiC devices available from commercial vendors are surveyed. Among them, HV SiC MOSFETs are the most developed. The MV power electronic equipment in distribution grids is summarized, and the role of SiC in these applications is analyzed. The microgrids, including conventional and asynchronous microgrids, are selected for detailed investigation considering the benefits of HV SiC that can be fully demonstrated in this application.

In the conventional microgrid, the benefits of using HV SiC in DER converters can be obtained both at the converter and system levels. At the converter level, the SiC-based DER converter has significant weight and size advantages compared with its Si-based counterpart, e.g., an 82.9% weight reduction and 73.2% size reduction can be achieved for a 1 MW, 13.8 kV PV interface converter using HV SiC devices. The SiC-based DER converters can work with a higher switching frequency (e.g., 3 times that of Si-based), and therefore have a higher control bandwidth. At the system level, the high control bandwidth results in power quality improvement, system stability enhancement, and better LVRT dynamic performance.

Similar to the conventional microgrid, HV SiC devices can also benefit asynchronous microgrid PCS at both the converter and system levels. At the converter level, the SiC-based PCS has significant benefits in weight and size (e.g., 94% weight reduction and 91% size reduction with SiC-based three-level 13.8 kV, 1 MW NPC, 85% weight reduction and 83% size reduction with SiC-based MMC, compared with a three-level Si NPC). The HV SiC-based PCS converters can work with a higher switching frequency (around 10 to 20 times higher than Si-based PCS converters), and therefore have a higher control bandwidth. At the system level, the high control bandwidth of the PCS converters can result in enhanced performance of the microgrids in terms of power quality, system stability, LVRT, transition between islanded mode and grid-connected mode, and black start capability. For power quality, SiC-based PCS can integrate the harmonic filtering capability and therefore eliminate the need for additional harmonic filters. On stability, the SiC PCS can isolate the impact of the grid impedance and enhance the system stability in grid-connected mode and operates as a stabilizer to enhance the stability in islanded mode. On LVRT, mode transition between grid-connected and islanded modes, and black start, the load in the microgrid can be supplied normally with the PCS, even during LVRT and mode-transition periods, and the black start can be easier. With the SiC-based PCS with much higher control bandwidth, better dynamic performance during LVRT, mode transition, and black start can be achieved compared to those of Si-based PCS.

References

[1] M Takeda, S Jochi. Development of adavanced solid state transfer switch using novel hybrid switch devices. *in Proc. ASDCOM*, 2003: 535-540.

[2] J Haefner, B Jacobson. Proactive hybrid HVDC breakers: A key innovation for reliable HVDC grids. *CIGRE Symposium*, Bologna, 2011.

[3] A Abramovitz, K M Smedley. Survey of solid-state fault current limiters, *IEEE Trans. Power Electron.*, 2012, 27(6): 2770-2782.

[4] N G Hingorani, L Gyugyi. Understanding facts: Concepts

and technology of flexible ac transmission systems. New York: IEEE Press, 2000.

[5] P S Georgilakis, P G Vernados. Flexible ac transmission system controllers: An evaluation. *Materials Science Forum*, 2011, 670: 399-406.

[6] M Zadehbagheri, N A Azil, A Bagherinasab, et al. Performance evaluation of custom power devices in power distribution networks to power quality improvement: A review. *International Journal of Scientific & Engineering Research*, 2013, 4(5): 44-49.

[7] M Montero, E Cadaval, F Gonzalez. Comparison of control strategies for shunt active power filters in three-phase four-wire systems. *IEEE Trans. Power Electron.*, 2007, 22(1): 229-236.

[8] S Babaa, M Armstrong, V Pickert. Overview of maximum power point tracking control methods for PV systems. *Journal of Power and Energy Engineering*, 2014: 59-72.

[9] S B Kjaer, J K Pedersen, F Blaabjerg. A review of single-phase grid-connected inverters for photovoltaic modules. *IEEE Trans. Ind. Appl.,* 2005, 41(5): 1292-1306.

[10] F Blaabjerg, M Liserre, K Ma. Power electronics converters for wind turbine systems. *IEEE Energy Conversion Congress and Exposition (ECCE)*, 2011, 281-290.

[11] Z Q Zhu, H Jiabing. Electrical machines and power-electronic systems for high-power wind energy generation applications: Part I-market penetration, current technology and advanced machine systems. *COMPEL: The International Journal for Computation and Mathematics in Electrical and Electronic Engineering,* 2013, 32: 7-33.

[12] M Liserre, R Cardenas, M Molinas, et al. Overview of multi-MW wind turbines and wind parks. *IEEE Trans. Ind. Electron.*, 2011, 58(4): 1081-1095.

[13] S Ponnaluri, G Linhofer, J Steinke, et al. Comparison of single and two stage topologies for interface of BESS or fuel cell system using the ABB standard power electronics building blocks. *European Conference on Power Electronics and Applications*, 2005: 1-9.

[14] EPRI. EPRI-DOE handbook of energy Storage for transmission & distribution applications. 2003. https://www.sandia.gov/ess-ssl/publications/ESHB%201001834% 20reduced%20size.pdf.

[15] F Blaabjerg, Z Chen, S Kjaer. Power electronics as efficient interface in dispersed power generation systems. *IEEE Trans. Power Electron.,* 2004, 19(5): 1184-1194.

[16] J Carrasco, L Franquelo, J Bialasiewicz, et al. Power-electronic systems for the grid integration of renewable energy sources: A survey. *IEEE Trans. Ind. Electron.,* 2006, 53(4): 1002-1016.

[17] I Alan, T A Lipo. Induction machine based flywheel energy storage system. *IEEE Trans. Aerospace and Electronic systems*, 2003, 39(1): 151-163.

[18] R H Lasseter. Microgrids. *IEEE Power Engineering Society Winter Meeting*, 2001: 146-149.

[19] S Backhaus, G W Swift. DOE DC microgrid scoping study: Opportunities and challenges. *in Proc. ICDCM*, 2005: 43-44.

[20] R Majunder, A Gosh, G Ledwich. Power management and power flow control with back-to-back converters in a utility connected microgrid. *IEEE Trans. Power Systems*, 2010, 25(2): 821-834.

[21] R Salcedo, A Bokhari, M Diaz-Aguilo, et al. Benefits of a nonsynchronous microgrid on dense-load LV secondary networks. *IEEE Trans. Power Del.,* 2013, 31(3): 1076-1084.

[22] R Majumder. A hybrid microgrid with DC connection at back to back converters. *IEEE Trans. Smart Grid,* 2014, 5(1): 251-259.

[23] S Xu, A Q Huang, R Burgos. Review of solid-state transformer technologies and their application in power distribution systems. *IEEE Journal of Emerging and Selected Topics in Power Electronics*, 2013, 1: 186-198.

[24] J Kolar, G Ortiz. Solid-state-transformers: Key components of future traction and smart grid systems. *Proceedings of the International Power Electronics Conference ECCE Asia (IPEC)*, May. 2014.

[25] Traction transformation: A power-electronic traction transformer (PETT). *ABB Review*, 2012, 1: 11-17.

[26] R Raju, R Steigerwald, M Dame. High voltage, high frequency silicon carbide power electronic building blocks. GE report. Available: https://www.nist.gov/system/files/documents/pml/high_megawatt/Approved-Raju-DoE_NIST_HMW_VSD_GE_raju.pdf.

[27] D Das, R Kandular, J Munoz, et al. An integrated controllable network transfomer-hybrid active filter system. *IEEE Trans. Ind. Appl.*, 2015, 51(2): 1692-1701.

[28] S Zheng, J Wang, F Yang, et al. A DC controller for continuous variable series reactor. *IEEE Energy Conversion Congress and Exposition* (*ECCE*), 2015: 5786-5793.

[29] J Wang. Design, characterization, modeling and analysis of high voltage silicon carbide power devices. North Carolina: North Carolina State Univ., 2010.

[30] Q Zhang, R Callanan, M K Das, et al. SiC power devices for microgrids. *IEEE Trans. Power Electron.*, 2010, 25: 2889-2896.

[31] A Hefner, R Sei-Hyung, B Hull, et al. Recent advances in

high-voltage, high-frequency silicon-carbide power devices. *Industry Applications Conference IAS Annual Meeting*, 2006: 330-337.

[32] SiC power devices and modules. Rohm Semiconductor Co., Appl. Note 13103EAY01, Jun. 2013. Available: https://d1d2qsbl8m0m72.cloudfront.net/en/products/databook/applinote/discrete/sic/common/sic_appli-e.pdf.

[33] J W Palmour. Future high voltage silicon carbide power devices. Wolfspeed Inc., *Workshop on Future Large CO2 Compression Systems*, Rep. Mar. 2009.

[34] D Grider, A Agarwal, S H Ryu, et al. Advanced SiC power technology for high megawatt power conditioning. *Wolfspeed Inc., High Megawatt Power Conditioning System Workshop*, Rep. May. 2012.

[35] D Grider, M Das, A Agarwal, et al. 10 kV/120 A SiC DMOSFET half H-bridge power modules for 1 MVA solid state power substation. *Electric Ship Technologies Symposium (ESTS)*, 2011: 131-134.

[36] M K Das, J J Sumakeris, B A Hull, et al. High power, drift-free 4H-SiC PiN diodes. *IEEE Lester Eastman Conference on High Performance Devices*, 2004: 236-240.

[37] R Singh. Ultra-high voltage SiC power devices for reduced power electronics complexity. GeneSiC Semiconductor. Available: https://www.arpa-e.energy.gov/sites/default/files/documents/files/SolarADEPT_Workshop_NxtGenPwr_Singh.pdf.

[38] USCi Custom Products. Available: https://www.ecomal.com/fileadmin/Datenblaetter/USCi/Leaflet/USCi_Leaflet.pdf.

[39] J Hostetler, P Alexandrov, X Li, et al. 6.5 kV Silicon carbide enhanced mode JFETs for high voltage DC link applications. https://www.sandia.gov/ess-ssl/docs/pr_conferences/2014/Thursday/PosterSession8/12_Hostetler_John_ENHANCED_MODE_JFETS_Poster.pdf.

[40] J W Palmour, L Cheng, V Pala, et al. Silicon carbide power MOSFETs: Breakthrough performance from 900 V up to 15 kV. *2014 IEEE 26th International Symposium on Power Semiconductor Devices & IC's (ISPSD)*, Waikoloa, HI, USA, 15-19 June 2014.

[41] J B Casady, T McNutt, D Girder, et al. Medium voltage SiC R&D update. Apr. 2016. https://www.nist.gov/system/files/documents/pml/high_megawatt/Wolfspeed-Cree-SiC-Pwr-NIST-wkshp-Apr2016_SHORT.pdf.

[42] R Sei-Hyung, K Sumi, B Hull, et al. 10 kV, 5 A 4H-SiC power DMOSFET. *IEEE International Symposium on Power Semiconductor Devices and IC's (ISPSD)*, 2006: 1-4.

[43] J Wang, T Zhao, J Li, et al. Characterization, modeling, and application of 10-kV SiC MOSFET. *IEEE Trans. Electron Devices*, 2008, 55: 1798-1806.

[44] A Huang. FREEDM system: A vision for the future grid. *Power and Energy Society General Meeting*, 2010: 1-4.

[45] Q Zhang, M Das, J Sumakeris, et al. 12-kV p-channel IGBTs with low on-resistance in 4H-SiC. *IEEE Trans. Electron Device*, 2008, 29: 1027-1029.

[46] R Sei-Hyung, C Capell, C Lin, et al. High performance, ultra high voltage 4H-SiC IGBTs. *Energy Conversion Congress and Exposition (ECCE)*, 2012: 3603-3608.

[47] Y Yonezawa, T Mizushima, K Takenaka, et al. Low V/f and highly reliable 16 kV ultrahigh voltage SiC flip-type n-channel implantation and epitaxial IGBT. *IEEE International Electron Devices Meeting (IEDM),* 2013: 661-664.

[48] J Hostetler, X Li, P Alexandrov, et al. 6.5 kV Silicon Carbide JFETs siwtch module for high density power conversion system. *EESAT Technical Conference*, Sep. 2015.

[49] J Bendel, X Li. Using “normally on” JFETs in power system. *Bodo's Power Systems*, 2015: 40-43.

[50] J Nakashima, A Fukumoto, Y Obiraki, et al. 6.5-kV full SiC power module (HV100) with SBD-embedded SiC-MOSFETs. *in PCIM Europe*, 2018: 441-447.

[51] N Soltau. 3.3 kV full SiC MOSFETs: Towards high-performance traction inverters. *Bodo's Power Systems*, 2018: 22-24.

[52] Propulsion systems using 3.3-kV all-SiC devices. https://www.toshiba.co.jp/infrastructure/en/news/20190314.htm.

[53] R Takayanagi, K Taniguchi, M Hoya, et al. 3.3 kV power module for electric distribution equipment with SiC trench-gate MOSFET. *in ICEP*, 2019: 83-87.

[54] Y Sekino, T Tsuji, T Shiigi, et al. 3.3 kV all SiC module with 1st generation trench gate SiC MOSFETs for traction inverters. *in PCIM Europe*, 2020: 98-103.

[55] B Singh, K Al-Haddad, A Chandra. A review of active filters for power quality improvement. *IEEE Trans. Ind. Electron.*, 1999, 46(5): 960-971.

[56] J Sun. Impedance based stability criterion for grid-connected inverters. *IEEE Trans. Power Electron.*, 2011, 26(11): 3075-3078.

[57] O Mahela, N Gupta, M Khosravy, et al. Comprehensive overview of low voltage ride through methods of grid integrated wind generator. *IEEE Access*, 2019, 7: 99299-99326.

[58] M Aboukheili, M Shahabi, Q Shafiee, et al. Seamless transition of microgrids operation from grid-connected to islanded mode. *IEEE Trans. Smart Grid*, 2020, 11(3): 2106-2114.

[59] F Qiu, J Wang, C Chen, et al. Optimal black start resource allocation. *IEEE Trans. Power Systems*, 2016, 31(3): 2493-2494.

[60] S Ji, S Zheng, F Wang, et al. Temperature-dependent characterization, modeling and switching speed limitation analysis of third generation 10 kV SiC MOSFET. *IEEE Trans. Power Electron.*, 2018, 33(5): 4317-4327.

[61] S Ji, M Laitinen, X Huang, et al. Short circuit characterization and protection of 10 kV SiC MOSFET. *IEEE Trans. Power Electron.*, 2019, 34(2): 1755-1764.

[62] L Zhang, S Ji, S Gu, et al. Design considerations for high-voltage-insulated gate drive power supply for 10-kV SiC MOSFET applied in medium-voltage converter. *IEEE Trans. Ind. Electron.*, DOI: 10.1109/TIE.2020.3000131 (early access).

[63] J Palmer, S Ji, X Huang, et al. Improving voltage sensor noise immunity in a high voltage and high dv/dt environment. *IEEE Applied Power Electronics Conference and Exposition* (*APEC*), 2020: 107-113.

[64] S Ji, X Huang, L Zhang, et al. Medium voltage (13.8 kV) transformer-less grid-connected DC/AC converter design and demonstration using 10 kV SiC MOSFETs. *IEEE Energy Conversion Congress and Exposition (ECCE)*, 2019: 1953-1959.

[65] S Ji, L Zhang, X Huang, et al. A novel voltage balancing control with dv/dt reduction for 10-kV SiC MOSFET-based medium voltage modular multilevel converter. *IEEE Trans. Power Electron.*, 2020, 35(11): 12533-12543.

[66] D Li, S Ji, X Huang, et al. Controller development of an asynchronous microgrid power conditioning system (PCS) converter considering grid requirements. *IEEE Applied Power Electronics Conference and Exposition* (*APEC*), 2020: 616-621.

[67] J Palmer, S Ji, X Huang, et al. Testing and validation of 10 kV SiC MOSFET based 35 kVA MMC phase-leg for medium voltage (13.8 kV) grid. *IEEE Energy Conversion Congress and Exposition (ECCE)*, 2019: 2001-2006.

Fred Wang received the B.S. degree from Xi'an Jiaotong University, Xi'an, China, in 1982, and the M.S. and Ph.D. degrees from the University of Southern California, Los Angeles, in 1985 and 1990, respectively, all in electrical engineering.

He was a research scientist in the Electric Power Lab, University of Southern California, from 1990 to 1992. He joined the GE Power Systems Engineering Department, Schenectady, NY, as an application engineer in 1992. From 1994 to 2000, he was a senior product development engineer with GE Industrial Systems, Salem, VA. From 2000 to 2001, he was the manager of the Electronic and Photonic Systems Technology Lab, GE Global Research Center, Schenectady, NY, and Shanghai, China. In 2001, he joined the Center for Power Electronics Systems (CPES), Virginia Tech, Blacksburg, as a research associate professor and became an associate professor in 2004. From 2003, he also served as the CPES Technical Director. Since 2009, he has been with The University of Tennessee and Oak Ridge National Lab, Knoxville, TN, as a professor and Condra Chair of Excellence in Power Electronics. He is a founding member of the NSF/DOE Engineering Research Center for Ultra-Wide-Area Resilient Electric Energy Transmission Networks (CURENT) led by the University of Tennessee. His research interests include power electronics and power systems. Dr. Wang is a fellow of the IEEE and a fellow of the US National Academy of Inventors.

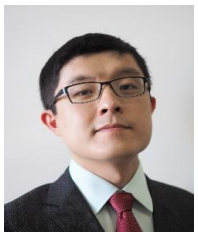

Shiqi Ji received the B.S. and Ph.D. degrees from Tsinghua University, Beijing, China, in 2010 and 2015, respectively, both in electrical engineering.

Since 2015, he joined the Ultra-Wide-Area Resilient Electric Energy Transmission Networks (CURENT), the University of Tennessee, Knoxville, TN, USA, and became a research assistant professor in 2019. Since 2020, he has been with Tsinghua University, Beijing, China, as an assistant professor. He has authored or co-authored more than 50 technical papers. His research interests include semiconductor device modeling, medium-voltage and high-power converter design, high-voltage SiC device characterization and application techniques, and grid-connected converter design.